Drug Design, Development and Therapy

Dovepress

open access to scientific and medical research

Open Access Full Text Article

ORIGINAL RESEARCH

Trimetazidine Alleviates Bleomycin-Induced Pulmonary Fibrosis by Targeting the Long Noncoding RNA CBR3-AS1-Mediated miRNA-29 and Resistin-Like Molecule alpha 1: Deciphering a Novel Trifecta Role of LncRNA CBR3-AS1/miRNA-29/FIZZ1 Axis in Lung Fibrosis

Abdullah R Alzahrani[1], Doaa I Mohamed[2], Hebatallah H Abo Nahas[3], Dalia Alaa El-Din Aly El-Waseef[4], Abdulmalik S Altamimi[5], Ibrahim H Youssef[6], Ibrahim Abdel Aziz Ibrahim[1], Soha MY Mohamed[7], Yasmine Gamal Sabry[7], Alaa H Falemban[1], Nasser Attia Elhawary[8], Ghazi A Bamagous[1], Mariusz Jaremko[9], Essa M Saied[10,11]

[1]Department of Pharmacology and Toxicology, Faculty of Medicine, Umm Al-Qura University, Makkah, Saudi Arabia; [2]Department of Clinical Pharmacology and Therapeutics, Faculty of Medicine, Ain Shams University, Cairo, Egypt; [3]Zoology Department, Faculty of Science, Port Said University, Port Said, Egypt; [4]Department of Histology and Cell Biology, Faculty of Medicine, Ain Shams University, Cairo, Egypt; [5]Department of Pharmaceutical Chemistry, College of Pharmacy, Prince Sattam Bin Abdulaziz University, Alkharj, Saudi Arabia; [6]Department of Chest Diseases, Faculty of Medicine, Al-Azhar University, Cairo, Egypt; [7]Physiology Department, Faculty of Medicine, Ain Shams University, Cairo, Egypt; [8]Department of Medical Genetics, College of Medicine, Umm Al-Qura University, Mecca, Saudi Arabia; [9]Smart-Health Initiative and Red Sea Research Center, Division of Biological and Environmental Sciences and Engineering, King Abdullah University of Science and Technology, Thuwal, Saudi Arabia; [10]Chemistry Department, Faculty of Science, Suez Canal University, Ismailia, Egypt; [11]Institute for Chemistry, Humboldt Universität Zu Berlin, Berlin, Germany

Correspondence: Essa M Saied, Institute for Chemistry, Humboldt Universität zu Berlin, Berlin, 12489, Germany, Email saiedess@hu-berlin.de

Introduction: Pulmonary fibrosis (PF) and tissue remodeling can greatly impair pulmonary function and often lead to fatal outcomes.

Methodology: In the present study, we explored a novel molecular interplay of long noncoding (Lnc) RNA CBR3-AS1/ miRNA-29/ FIZZ1 axis in moderating the inflammatory processes, immunological responses, and oxidative stress pathways in bleomycin (BLM)-induced lung fibrosis. Furthermore, we investigated the pharmacological potential of Trimetazidine (TMZ) in ameliorating lung fibrosis.

Results: Our results revealed that the BLM-treated group exhibited a significant upregulation in the expression of epigenetic regulators, lncRNA CBR3-AS1 and FIZZ1, compared to the control group ($P<0.0001$), along with the downregulation of miRNA-29 expression. Furthermore, Correlation analysis showed a significant positive association between lnc CBR3-AS1 and FIZZ1 ($R=0.7723$, $p<0.05$) and a significant negative association between miRNA-29 and FIZZ1 ($R=-0.7535$, $p<0.05$), suggesting lnc CBR3-AS1 as an epigenetic regulator of FIZZ1 in lung fibrosis. BLM treatment significantly increased the expression of Notch, Jagged1, Smad3, TGFB1, and hydroxyproline. Interestingly, the administration of TMZ demonstrated the ability to attenuate the deterioration effects caused by BLM treatment, as indicated by biochemical and histological analyses. Our investigations revealed that the therapeutic potential of TMZ as an antifibrotic drug could be ascribed to its ability to directly target the epigenetic regulators lncRNA CBR3-AS1/ miRNA-29/ FIZZ1, which in turn resulted in the mitigation of lung fibrosis. Histological and immunohistochemical analyses further validated the potential antifibrotic effects of TMZ by mitigating the structural damage associated with fibrosis.

Received: 9 February 2024
Accepted: 28 August 2024
Published: 5 September 2024

Discussion: Taken together, our study showed for the first time the interplay between epigenetic lncRNAs CBR3-AS1 and miRNA-29 in lung fibrosis and demonstrated that FIZZ1 could be a downregulatory gene for lncRNA CBR3-AS1 and miRNA-29. Our key findings demonstrate that TMZ significantly reduces the expression of fibrotic, oxidative stress, immunomodulatory, and inflammatory markers, along with epigenetic regulators associated with lung fibrosis. This validates its potential as an effective antifibrotic agent by targeting the CBR3-AS1/miRNA-29/FIZZ1 axis.

Keywords: lung fibrosis, long noncoding RNA CBR3-AS1, miRNA-29, FIZZ1, trimetazidine, histopathology

Graphical Abstract

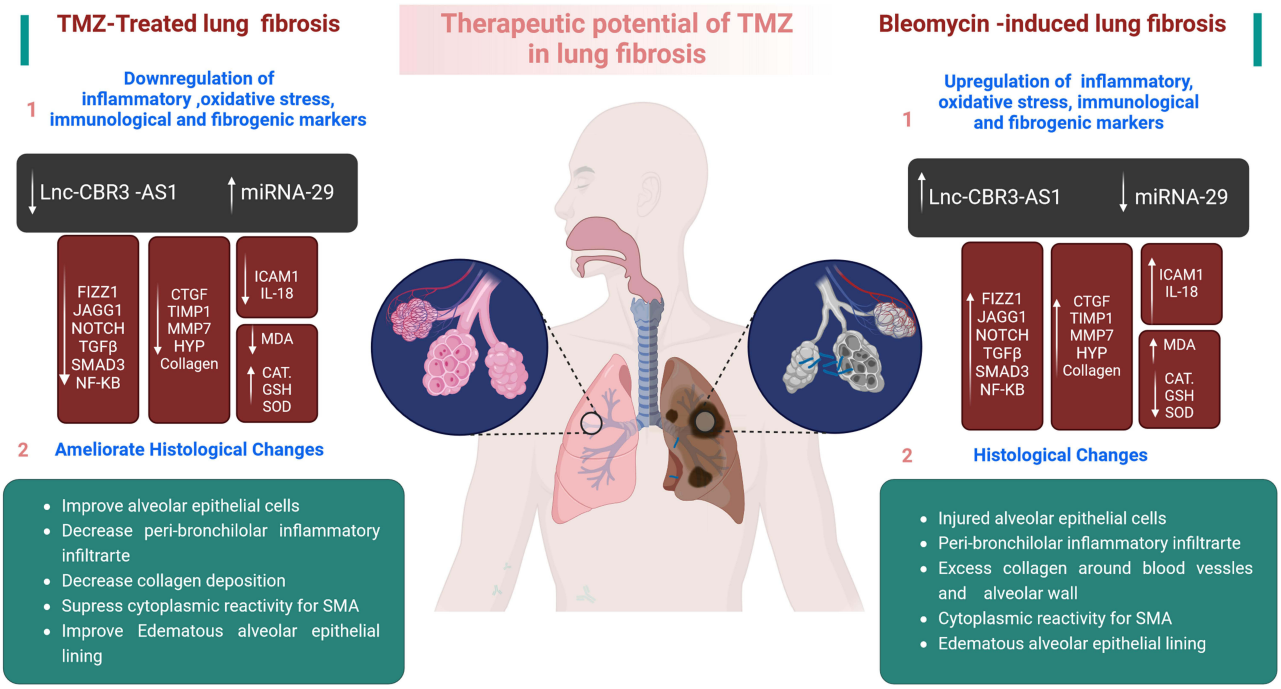

Introduction

Pulmonary fibrosis (PF), also referred to as lung fibrosis, presents a significant global health challenge with a high mortality rate and few effective treatment options. It is a progressive lung disease characterized by the gradual formation of scar tissue within the lung parenchyma, ultimately leading to respiratory failure and death.[1] The prevalence of IPF varies globally, with incidence rates ranging from 0.09 to 1.30 per 10,000 individuals and prevalence rates ranging from 0.33 to 4.51 per 10,000 individuals. It predominantly affects males aged over 50 years and shows considerable geographic diversity.[2] The pathogenesis of pulmonary fibrosis has redirected the focus from fibroblast-driven mechanisms to those centered on epithelial cells. This evolving perspective highlights that recurrent micro-injuries result in the dysfunction of alveolar type II epithelial cells (ATII). These dysfunctional ATII cells not only fail to sustain normal lung regeneration but also contribute to aberrant epithelial-mesenchymal crosstalk. Consequently, this promotes fibrotic processes over the regeneration of healthy lung tissue.[3,4] PF is a significant component of various interstitial lung disorders (ILDs), with idiopathic PF being particularly severe and life-threatening.[5] However, the precise origin of myofibroblast involvement in fibrosis remains unclear. Numerous studies have identified the Epithelial-Mesenchymal Transition (EMT) as a plausible contributor to fibrotic development.[6] EMT is a biological process that involves the conversion of epithelial cells to mesenchymal cells, resulting in enhanced migratory and invasive characteristics.[7] EMT

encompasses several key features, such as disruption of cell-cell interactions, reconfiguration of the actin cytoskeleton, and cell separation, leading to the transformation of epithelial cell layers into fibroblast-like cells, marked by increased motility and specific genetic marker expression.[8] Despite the availability of anti-inflammatory and immunosuppressive treatments, a complete cure for lung fibrosis remains a challenge. The most frequently used animal model to study PF is intratracheal instillation of the anticancer drug bleomycin (BLM).[9] BLM can produce reactive oxygen metabolites such as superoxide and hydroxyl radicals, which can initiate DNA damage by inducing strand cleavage.[10] This, in turn, may trigger lipid peroxidation, carbohydrate oxidation, alterations in prostaglandin synthesis and degradation in the lungs, and increased collagen synthesis in the pulmonary tissues. BLM-induced lung injury is characterized by a complex inflammatory process involving various immune cell types including macrophages, neutrophils, and lymphocytes.[11] Further, a considerable alternation in the expression of oxidative stress markers has been associated with BLM-induced lung injury including superoxide dismutase (SOD), catalase, and glutathione (GSH), as well as measures of lipid peroxidation such as malondialdehyde (MDA).[12]

Long non-coding RNAs (lncRNAs) are RNA sequences comprising over 200 nucleotides that play crucial roles in controlling transcription and regulating gene expression through epigenetic mechanisms and offer distinct advantages in the realm of epigenetic regulation.[13,14] The lncRNA CBR3-AS1, also known as plncRNA-1, is a lncRNA encoded on chromosome 21q22.12 with a transcriptional length of 749 nt and was initially found to be highly expressed in prostate cancer cells.[15] A study conducted by Liu et al shed light on the molecular mechanisms of lncRNA CBR3-AS1 in non-small cell lung cancer development.[16] The authors observed that lncRNA CBR3-AS1 was overexpressed in NSCLC tissues compared to adjacent normal tissues. Downregulation of lncRNA CBR3-AS1 levels led to a decrease in cell proliferation, migration, and invasiveness; hindered cell cycle progression; and promoted apoptosis in NSCLC cells. The lncRNA CBR3-AS1 has also emerged as a key player in Notch/Jagged1 and TGF-B1 components, which are pivotal in fibrotic processes.[17,18] Remarkably, a recent study showed that the lncRNA CBR3-AS1 is associated with the inhibition of miRNA-29-mediated cell invasion and migration in colorectal cancer cells.[19] This interconnectedness suggests that lncRNA CBR3-AS1 may act as a central node that coordinates communication between different targets of the lung fibrosis pathway and, therefore, may be a promising candidate for drug intervention in lung fibrosis. MicroRNAs (miRNAs) are a category of non-coding RNAs responsible for the regulation of gene networks. Previous studies have shown that systemic gene transfer of miRNA-29 results in the reduction of lung fibrosis in animal models.[20] Furthermore, in two distinct groups of patients with IPF, lower levels of miRNA-29 were associated with higher mortality rates when observed in peripheral blood. This finding suggests that individuals with decreased miRNA-29 concentration in their blood could potentially be identified as a target population for treatment strategies.[21] Previous studies have established that downregulation of miRNA-29 is associated with an increase in the expression of Smad and TGF-β.[20] This molecular cascade contributes significantly to pathological processes and cellular responses that underlie the development and progression of lung fibrosis.[20,22] This finding provides support for the exploration of miRNA-29-based treatments as potential approaches for managing IPF.

The induction of myofibroblast differentiation has been attributed to the presence of Inflammatory Zone 1 (FIZZ1), which is believed to trigger the Notch signaling pathway and contribute to the development of fibrosis.[23] The efficacy of FIZZ1 in upregulating the expression of the activated intracellular domain of Notch1 and its ligand Jagged1 has been established. The observed upregulation has been associated with increased levels of α-smooth muscle actin expression (α-SMA), which serves as an indicator of myofibroblast differentiation in the context of fibrosis.[24] The Jagged ligand/Notch receptor signaling pathway has been implicated in the regulation of epithelial function and the production of EMT during embryogenesis and cancer.[25] Fibrogenesis is primarily initiated by transforming growth factor-β (TGF-β), which is regulated by Smad-dependent or non-Smad pathways and is influenced by co-receptors and interaction networks.[26] The TGF signaling pathway is initiated in fibroblasts through the activation of TGF type I receptor kinase (ALK5).[27] The stimulatory effect of TGF-on fibrogenesis has been well-documented in both in vivo and in vitro studies. However, owing to the multifaceted nature of TGF activity, the development of antifibrotic medicines that specifically target the TGF axis poses significant challenges.[28] In recent years, hydroxyproline has garnered growing interest as a significant biomarker for PF, owing to its specific interaction with collagen.[29] Nuclear factor kappa B (NFκB) represents a group of dimeric transcription factors with the capacity to bind to DNA, thereby assuming a central role in regulating a wide array of

biological reactions that are triggered in response to cellular stress.[30] In lung fibrosis, NF-κB serves as a crucial metric for the initiation and progression of fibrotic changes within pulmonary tissue.[31]

Among the key regulatory factors coordinating immune cell migration are chemokines, a specialized category of cytokines known for their role in guiding immune cell trafficking via specific receptor interactions.[32] Interleukin (IL)-18, a member of the IL-1 gene family, functions as a proinflammatory cytokine and plays a role in both acquired and innate immunity.[33] The activation of T helper type 1 cells and induction of IL-2 production were observed upon stimulation with IL-18. Furthermore, the protein known as Intercellular Adhesion Molecule-1 (ICAM-1) belongs to the immunoglobulin superfamily and acts as a binding agent for lymphocyte function-associated antigen I alpha. It has been observed that ICAM-1 is significantly involved in inflammatory pulmonary conditions such as bronchial asthma and damage caused by hyperoxia-induced damage.[34] In the intricate network of molecules contributing to PF, the *MMP7* gene takes center stage. This gene encodes an ECM-degrading enzyme, a member of the matrix metalloproteinase (MMP) family, which plays a role in various biological processes including tissue remodeling and atherosclerosis progression. Interestingly, mice lacking MMP-7 exhibited non-functional crypts, emphasizing the importance of this gene in maintaining tissue integrity. Moreover, studies have demonstrated that MMP-7 plays a pivotal role in the induction of PF, as evidenced by the protection of MMP-7-deficient mice from lung injury caused by BLM exposure.[35,36]

Current therapies for PF aim to manage symptoms and slow disease progression. However, a definitive cure remains elusive. Lung transplantation is the only feasible treatment for individuals with advanced stages of lung fibrosis.[37] Trimetazidine (TMZ) is a commonly used anti-ischemic medication for the treatment of coronary artery disease, which inhibits the long-chain 3-ketoacyl coenzyme in the mitochondria, particularly thiolase.[38] Recent studies have shown that TMZ administration in the early stages can reduce the incidence and progression of cardiac fibrosis in rat models of diabetic cardiomyopathy, indicating that its benefits extend beyond cardiomyocytes.[39] Accordingly, TMZ may possess considerable pharmacological potential for the attenuation of PF by improving cellular metabolic processes by enhancing glucose oxidation and blocking the β-oxidation of fatty acids. Furthermore, TMZ exhibits anti-apoptotic properties by enhancing cellular autophagic capability and mitigating induced apoptosis.[40] This may help to maintain energy metabolism during ischemia, preserving cellular homeostasis and ionic pump function.[41] Remarkably, TMZ has been shown to substantially inhibit the TGF-1β/Smad/α-SMA signaling pathway in CCl4-induced hepatic fibrosis, leading to the attenuation of fibrosis and cell proliferation.[42] Taken together, these findings suggest that TMZ may possess a potential pharmacological effect against lung fibrosis by targeting several molecular cascades.

Based on the above-mentioned facts, there is a possible correlation between miRNA-29 and lncRNA CBR3-AS1 expression in lung fibrosis and FIZZ1-mediated Notch/Jagged1 pathway (Figure S1). In our continuous efforts to decipher novel therapeutic targets for human diseases,[43–51] we aimed to explore a novel molecular interplay of the lncRNA CBR3-AS1/ miRNA-29/ FIZZ1 axis in modulating the Notch/Jagged1/Smad3/TGF-ß1 pathway and unveil how this molecular cascade jointly regulates the development and progression of lung fibrosis. Furthermore, we explored the pharmacological potential of TMZ to ameliorate lung fibrosis by targeting the proposed lncRNA CBR3-AS1/ miRNA-29/ FIZZ1 axis.

Material and Methods

Chemicals and Drugs

The study utilized BLM, trimetazidine, and thiopental sodium obtained from the Sigma Chemical Company (Cairo, Egypt).

Animals

All animal procedures were approved by the Institutional Animal Ethics Committee of Ain Shams, University Faculty of Medicine (FMASU R212/2023). Twenty-eight male Wistar rats weighing 150 g and 200 g were acquired from the National Research Institute in Cairo, Egypt. The animals were housed in a temperature-controlled animal facility with a 12-hour light/dark cycle. Before beginning the experimental protocol, the rats were given a one-week adaptation period to familiarize themselves with their new surroundings. This was done to ensure that ethical guidelines were followed and that the animals were in the best possible condition for the duration of the study.

Experimental Design

To create a rat model of PF, 5 mg/kg BLM sulfate salt was dissolved in 0.1 mL of normal saline and instilled into the trachea. The rats rotated vertically to ensure proper dispersion within the lung tissues. Anesthesia was achieved by intraperitoneal injection of 20 mg/kg of thiopental sodium. A midline incision was made in the neck to expose the trachea for BLM administration. The incision was then surgically sutured and a topical application of 2% sodium fusidate was applied to the wound.[52] Twenty-eight male Wistar rats were randomly assigned to one of four groups (n=7).

1) Control group: Rats were treated with 0.1 mL of normal saline by intratracheal instillation.
2) BLM-treated group: Rats were given BLM (5 mg/kg, diluted in 0.1 mL of normal saline) via intratracheal instillation.[53–55]
3) TMZ-treated group: Rats were orally treated with TMZ at a dosage of 15 mg/kg/day for four weeks.
4) TMZ + BLM group: Rats were treated with BLM (5 mg/kg) via intratracheal instillation, followed by the oral administration of TMZ at a dose of 15 mg/kg/day for four weeks.[56]

The health and activity of rats were monitored throughout the experiment. After the experiment, blood and lung tissue samples were collected from all the rats for biochemical, histopathological, and immunohistochemical analyses. The purpose of this analysis was to evaluate changes in lung tissue at the molecular and cellular levels due to experimental interventions (Figure 1). Blood samples were obtained from the retro orbital region and collected into plain tubes. Subsequently, the samples were centrifuged at 3000 rpm for 15 min to separate the serum, which was then stored at −80°

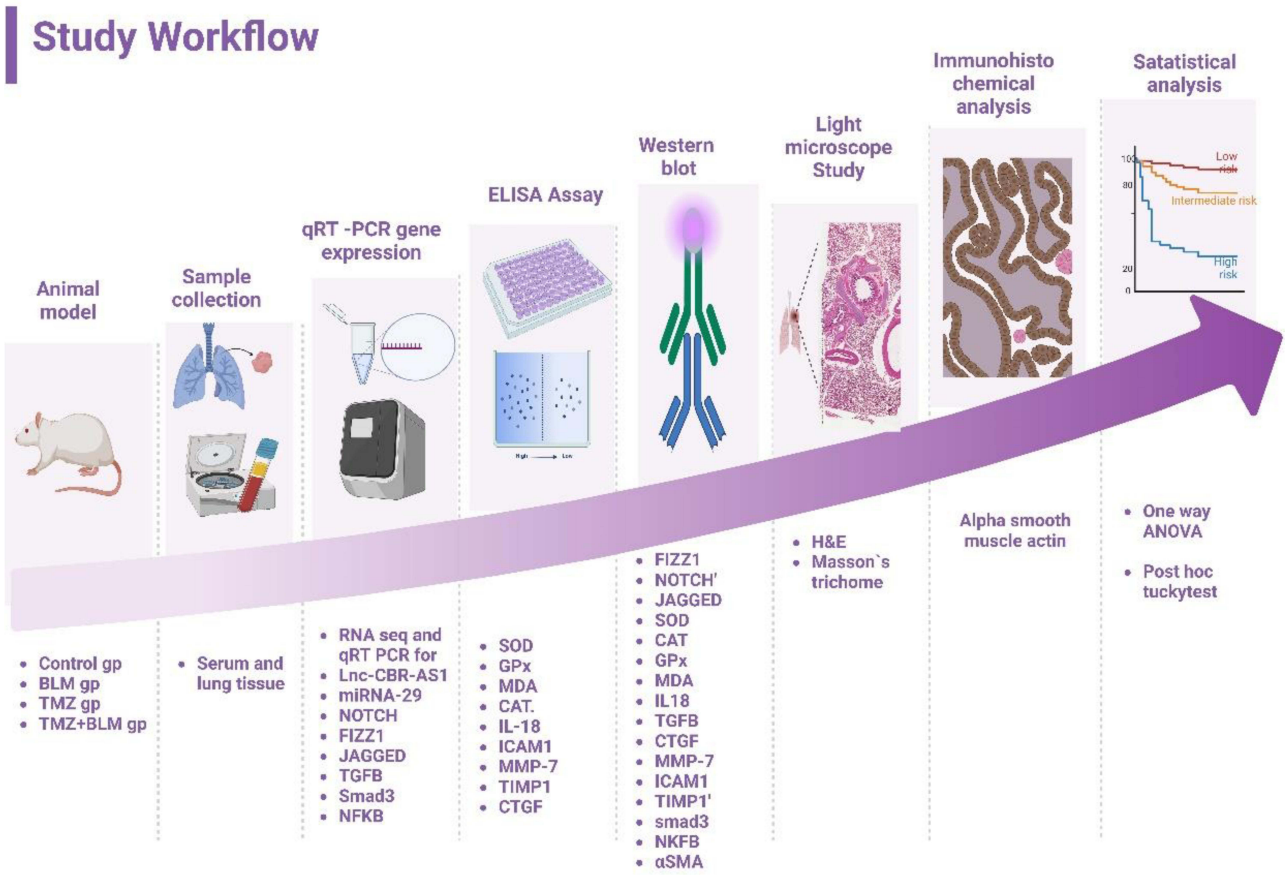

Figure 1 The designed workflow aims to elucidate the molecular interplay of the LncRNA CBR3-AS1/miRNA-29/FIZZ1 axis in modulating lung fibrosis, and the potential protective effects of TMZ. The workflow details the following key steps: identification of target interactions through experimental validation, functional assays to assess the impact on cellular processes relevant to fibrosis, and comprehensive analysis of gene expression changes in lung tissue samples to understand the regulatory mechanisms involved. Finally, histological and immunochemical assessments of lung tissues to examine the architectural structure of lung tissues.

C for subsequent biochemical analysis. The lungs of all rats were excised through an incision in the chest area, followed by two washes with a cold saline solution. Right lung tissues were preserved in 10% formalin solution for microscopic examination. Tissue homogenization was performed to analyze the chemical properties of the left lung tissues tissue.

RNA Isolation from Lung Sample

We retrieved lncRNAs that regulate miRNAs with many target genes involved in lung fibrosis, using the InCeDB database (http://gyanxetbeta.com/lncedb/index.php). We selected LncRNA-CBR-AS1 related to be involved in cell proliferation and lung fibrosis. Total RNA was extracted from lung tissue samples using the RNeasy Mini Kit (Qiagen, Hilden, Germany), according to the manufacturer's instructions. The concentration of RNA in each sample was measured using a NanoDrop 1000 spectrophotometer (Thermo Fisher Scientific, USA). A ratio of absorbance at A260/A280 of 1.8–2.1 was generally accepted as"pure"for RNA. Reverse transcription was performed using MiScript II RT PCR kits (Qiagen catalog no. 218161, Hilden, Germany) according to the manufacturer's protocol. The reverse transcription reactions were stored at −20°C prior to real-time PCR.

Lnc-CBR-AS1 Expression Analysis

Lnc-CBR-AS1 was quantified by adding 10μL 2x RT2 SYBR Green ROX qPCR Mastermix, followed by RT2 lncRNAq PCR Assay for Rat Hoxb1 (XM_001081344) (cat no: 330001, ID PPR45880A). 2μL of template ecDNA and RNase-free water were added to a final volume of 20μL. The ACTB_1_SG Quanti Tect Primer Assay (NM_001101) was used as a housekeeping gene for the normalization of our raw data and compared with a reference sample. The PCR program for the relative quantification of lncRNAs was as follows: denaturation at 95°C for 10 min, followed by 45 cycles of denaturation 15sat 95°C; then annealing 30sat 55°C and extension for 30s. Relative quantification of serum RNAs was calculated using Schmittgen and Livak (2008) for each examined sample. The threshold cycle (Ct) value of each sample was calculated using the Rotor Gene real-time PCR detection system (Qiagen, Hilden, Germany). The melting curve was analyzed to confirm the specificity of the amplicons for qPCR.

Assessment of mi-RNA 29 by Real-Time PCR

Tissue Homogenization: Tissue samples were suspended in a 2.0 mL screw cap tube containing 200 μL of phosphate buffer saline (PBS), a single 5 mm stainless steel bead (Qiagen) was added to each tube, and the samples were homogenized at maximum speed (30 Hz) for 2 min using the Qiagen Tissue Lyser system. Following homogenization, the samples were spun for 1 min at maximum speed to reduce foaming, and the homogenate was applied to a filter column for RNA extraction. miRNA and total mRNA extraction and purification: miRNA and total mRNA were extracted using a miRNeasy Mini Kit (Qiagen, Hilden, Germany) according to the manufacturer's protocol. Reverse transcription cDNA was synthesized by reverse transcription reaction using the miScript II RT Kit (Qiagen, Hilden, Germany). miRNA expression analysis. The quantification of miR-29 levels was performed using the SYBR-Green fluorescent-based primer assay (hsa-miR-29: cat no: MS00003528), and Hs_RUN6-2_11 (cat no: MS00033740) was used as a housekeeping gene for normalization. qPCR was performed using a 5-plex Rotor Gene PCR System (Qiagen). The reaction mixture (20 μL) consisted of 2×QuantiTect SYBR Green PCR master mix, 10× Miscript universal primers, 2 μL primer assay, and 50 pg^{-3} ng cDNA. Both targets were amplified in duplicates for each sample. The thermal protocol consisted of 15 min of hot start Taq DNA polymerase activation at 95◦C followed by 40 cycles of denaturation at 94 ◦C for 15 min, primer annealing for 30s at 55 ◦C and extension at 70◦C for 30s). The 2ΔΔCt method was used to analyze miR-145 expression levels, using RUN6 as an endogenous reference control for normalization purposes.

Assessment of Inflammatory Biomarkers in Lung Tissue by Real-Time PCR

To investigate the impact of TMZ on potential markers (FIZZ1, Jagged1, Notch, TGFβ, Smad3, and NFKB) in lung tissue, lung samples from the left lung were stored at −80°C. Total RNA was extracted using an RNeasy Mini Kit (catalog no. 74104) and reverse-transcribed using an iScript One-Step RT-PCR Kit with SYBR® Green (catalog no. D045-1 and D045-2) was purchased from Qiagen (Hilden, Germany). PCR primers were designed according to standard guidelines, with a length ranging from 18 to 25 nucleotides and a GC percentage ranging between 40% and 65%

Table 1 The List of Primer Pairs Used in qRT-PCR Analysis for the Selected Genes of Their miRNA Expression

Gene Name	Forward Primer	Reverse Primers
Lnc CBR3-AS1	F5′-CAATAGGGAAGCAGAGGGAGAA-3′	R5′-TTAGAGATTCCTACAGACCCAGGTC-3′
miRNA-29	F5'-GTGGGTAAGGGAGAGGGAAG-3'	R 5-'ACAT-TGCCTTCTCCCCAAAG-3`
FIZZ1	F 5'- CAACAGGATGAAGACTGCAACCT −3'	R 5'- GGGACCATCAGCTAAAGAAG −3'.
NOTCH	F 5'-CACCCATGACCACTACCCAGTT-3'	R 5'- CCTCGGACCAATCA-GAGATGTT −3'
JAGGED1	F 5'-AACTGGTACCGGTGCGAA −3'	R 5'-TGATGCAAGATCTCCCT-GAAAC-3'
TGFβ	F 5'- TGATACGCCTGAGTGGCTGTCT −3'	R 5'- CACAAGAGCAGTGAGCGCTGAA −3'
SMAD3	F 5'-GCTTTGAGGCTGTCTACCAGCT-3'	R 5'-GTGAGGACCTTGACAAGCCACT-3'
NFkB	F 5'-GCCTCTTCTCATTCCTGCTTG-3'	R5'-CTGATGAGAGGGAGGCCATT-3'

(Table 1). The primers and primer pairs were designed to avoid internal secondary structures and complementarity at the 3' end with careful consideration. To optimize reaction efficiency and specificity, the primer concentration varied from 100 to 500 nM, and a final concentration of 300 nM per primer was generally effective for most reactions. To achieve the best results, it is recommended to use equal concentrations of each primer, while restricting the amplicon size to a range of 50–200 base pairs. For the template, the suggested input quantities range from 1 pg to 100 ng of total RNA or 10 fg to 100 ng of polyA(+) RNA. First-strand synthesis was performed between 40°C and 52°C, with the best outcomes observed at 50°C for 10 min. Higher temperatures may lead to difficulties in detecting non-specific amplification artifacts. Prior to use, all components except iScript reverse transcriptase were thawed at room temperature. Mix gently and centrifuge at 4°C to ensure proper collection of contents at the bottom of the tube, and then chill on ice. To minimize pipetting errors and enhance assay accuracy in quantitative PCR applications, it is essential to prepare a reaction cocktail by combining all necessary constituents, except for the sample template (total RNA), and then equally distribute aliquots into individual reaction tubes. Finally, the target sample was added in volumes ranging from 5 to 10 µL to improve the assay precision. For the replicated samples, a master mix was assembled by incorporating a single addition of the sample template.

Biochemical Measurements

Assessment of Serum Immunological Markers

Blood samples (1 mL) were collected from the rat hearts and placed in centrifuge tubes (1.5 mL). The serum was extracted by centrifuging the blood for 10 min at 3000 rpm at 4 °C. The serum IL18 and ICAM1 levels were detected using an ELISA kit (Jianglai Biological Technology, Shanghai, China) according to the manufacturer's instructions.

Assessment of Serum Oxidative Stress Markers

The serum malondialdehyde (MDA), superoxide dismutase (SOD), catalase (CAT), and glutathione peroxidase (GPx) levels were determined using advanced laboratory techniques. Enzyme-linked immunosorbent assay (ELISA) was employed for the assessment, utilizing specific assay kits for each biomarker. The MDA levels were quantified using the OxiSelect "TBARS; Thiobarbituric Acid Reactive Substances" assay kit from CELL BIOLABS, USA. GPx activity was measured using a GPx assay kit (Cayman Chemical, Ann Arbor, MI, USA). SOD levels were quantified using an assay kit (catalog no. MBS266897; BioSource).

Assessment of Serum and Tissue Fibrogenic Markers

Fibrogenic markers, including Matrix Metalloproteinase-7 (MMP-7), Tissue Inhibitor of Metalloproteinase-1 (TIMP-1), and Connective Tissue Growth Factor (CTGF), were assessed using enzyme-linked immunosorbent assay (ELISA) kits (R&D Systems, Minneapolis,),)SAin according to the manufacturer's specifications. The evaluation protocol strictly adhered to the guidelines. Additionally, the fibrogenic impact in the lung tissue was quantified by measuring the hydroxyproline content, following the method outlined in the hydroxyproline assay kit sourced from Sigma-Aldrich Co. (Germany). The absorbance was recorded at 560 nm using a microplate reader. To determine lung collagen content, hydroxyproline assay results were used in the calculation:

Lung collagen content = Hydroxyproline content (13.517) The results were expressed as μg of collagen per milligram of wet lung tissue.[57] ELISA kits from R&D Systems were used for the measurements following the manufacturer's protocol.

Western Blot Study

The immunoblotting assay was employed for protein quantification and analysis. Homogenized lung tissue samples were processed using the ReadyPrep™ Protein Extraction Kit (Bio-Rad, Cat. #163-2086), For each sample, 20 μg of protein was combined with an equivalent volume of 2x Laemmli sample buffer. This buffer comprised 4% SDS, 10% 2-mercaptoethanol, 20% glycerol, 0.004% bromophenol blue, and 0.125 M Tris-HCl (pH 6.8) (Bio Basic Inc., Cat. #SK3041). To denature the proteins, the mixture was heated at 95°C for 5 minutes before being loaded onto a polyacrylamide gel (TGX Stain-Free™ Cat # 161–0181) for electrophoresis. Post-electrophoresis, the proteins were transferred to a PVDF membrane using the BioRad Trans-Blot Turbo system. The transfer sandwich, comprising filter paper, the PVDF membrane, the gel, and another filter paper, was assembled and placed in the transfer tank with 1x transfer buffer (25 mM Tris, 190 mM glycine, and 20% methanol). The transfer was executed at 25 V for 7 minutes To block non-specific binding, the membrane was incubated in TBST buffer at room temperature for 1 hour. The membrane was probed with targeted primary antibodies, including CTGF/CCN2 Antibody (NB100-724, Novus Biologicals, USA), IL-18 (11E5) (Santa Cruz Biotech., Cat. #sc-52012), SOD-2 (A-2) (Santa Cruz Biotech., Cat. #sc-133134), MDA-7 (Y14) (Santa Cruz Biotechnology, Cat. #sc-80184), Catalase (H-9) (Santa Cruz Biotech., Cat. #sc-27180), Jagged1 (E-12) (Santa Cruz Biotech., Cat. #sc-390177), Glutathione Reductase (B-12) (Santa Cruz Biotech, Cat. #sc-133159), FIZZ1/RELM Alpha Antibody (NBP2-29355, Novus Biologicals, USA), ICAM-1 (G-5) (Santa Cruz Biotech., Cat. #sc-8439), TGFβ1 (3C11) (Santa Cruz Biotech., Cat. #sc-130348), NFκB (Santa Cruz Biotech., Cat. # sc-8008), Smad3 (38-Q) (Santa Cruz Biotech., Cat. #sc-101154), MMP7 Polyclonal Antibody (Protein tech, Cat. #10374-2-AP), NOTCH1 Polyclonal Antibody (Elabscience, Cat. #E-AB-12815, USA), α-Smooth Muscle Actin Antibody (Cell Signaling Tech., Cat. #14968, USA), and TIMP1 (D10E6) mAb (Cell Signaling Tech., Cat. #8946, USA). For protein detection, primary antibodies were diluted in TBST and incubated overnight at 4°C. Chemiluminescence was developed using Clarity™ Western ECL Substrate (Bio-Rad, Cat. #170-5060) and captured with a CCD camera. Protein band intensities were analyzed and normalized against beta-actin using the ChemiDoc MP system.

Histological Studies

Light Microscopic Study

After obtaining the right lung from all rats, it was preserved in a solution of neutral-buffered formaldehyde (10%) and placed in paraffin blocks. We cut 5-μm serial sections and stained them with hematoxylin and eosin (H&E) and Masson's trichrome. The sections were analyzed using an Olympus CKX41 light microscope (Olympus Corporation, Tokyo, Japan) to detect microscopic changes or tissue fibrosis. We evaluated histological changes in five randomly chosen fields in all sections, but not consecutively.[58]

Immunohistochemical Analysis

To detect lung fibrosis, we used an immunohistochemical method with an avidin-biotin-peroxidase technique (Lab Vision, CA, USA) to test for the α-SMA antibody. We diluted it at 1:800 and left it for one and a half hours. Next, the secondary antibody (DAKO, Denmark) was added to the sections for 30 min. The reaction was developed for 10 min using DAB solution (purchased from DAKO, Denmark), and the slides were counterstained with Mayer's hematoxylin. We prepared a positive control using smooth muscles with the same protocol and a negative control with the same protocol, but without using the primary antibody.[59]

Morphometric Study

The Histology Department at Ain Shams University utilized a Leica Qwin 500 computer system for image analysis to measure the following parameters.

- Average thickness of the interalveolar septum in H&E-stained sections was measured in micrometers (μm) using a ×40 power lens.
- Average percentage of collagen fibers in Masson's trichrome-stained sections using a ×40 power lens.
- Average percentage of α-SMA positive immunostained sections using a ×20 power lens.

Statistical Analysis

We used two software programs for statistical analysis: GraphPad Prism version 5.0 (2007) (Inc., CA, USA) and SPSS 21 program (IBM Inc., Chicago, IL, USA). To compare statistical differences between groups, a one-way analysis of variance (ANOVA) followed by a post-hoc Tukey's test was conducted. SPSS 21 was used to calculate the mean values and standard deviations (SD) of the histological parameters, and another ANOVA test was conducted to compare variations between different groups. The significance level was determined based on the p-value, where a p-value less than 0.05 was considered statistically significant and a p-value less than 0.0001 was highly significant. GraphPad StatMate software version 1.01i Jan was used to determine the optimal sample size. To perform the morphometric analysis, we measured various parameters in five distinct fields from two consecutive sections of each animal within each group. The mean and standard deviation (SD) of these measurements were computed using SPSS 21 software (IBM Inc., Chicago, IL, USA). To compare the results, we applied a one-way Analysis of Variance (ANOVA) with a subsequent Least Significant Difference (LSD) post-hoc test. The significance of the data was assessed based on the calculated *P*-value, where a value of $P < 0.05$, was considered indicative of statistical significance.

Results

TMZ Upregulated the Expression of miRNA-29 Gene by Targeting the Epigenetic Regulator Lnc CBR3-AS1 in BLM-Induced Lung Fibrosis

First, we explored the effect of epigenetic regulators on lung fibrosis by assessing the expression of lnc CBR3-AS1 in a BLM-induced lung fibrosis model. The long noncoding RNA CBR3-AS1 plays a vital role in facilitating the epithelial-mesenchymal transition and regulating the signaling pathways of both TGF-β1 and Notch/jagged1. As shown in Figure 2, BLM treatment significantly ($P<0.0001$) increased the expression of lnc CBR3-AS1 as compared to that in the control group. These results indicate that lnc CBR3-AS1 plays a molecular epigenetic regulatory role not only in lung cancer, but also in lung fibrosis. We next assessed the effect of TMZ administration by evaluating the expression levels of lnc CBR3-AS1 in the TMZ-treated control and TMZ-treated model groups. The results indicated that TMZ had no significant effect on lnc CBR3-AS1 expression levels as compared to the control group, while it demonstrated a significant attenuation

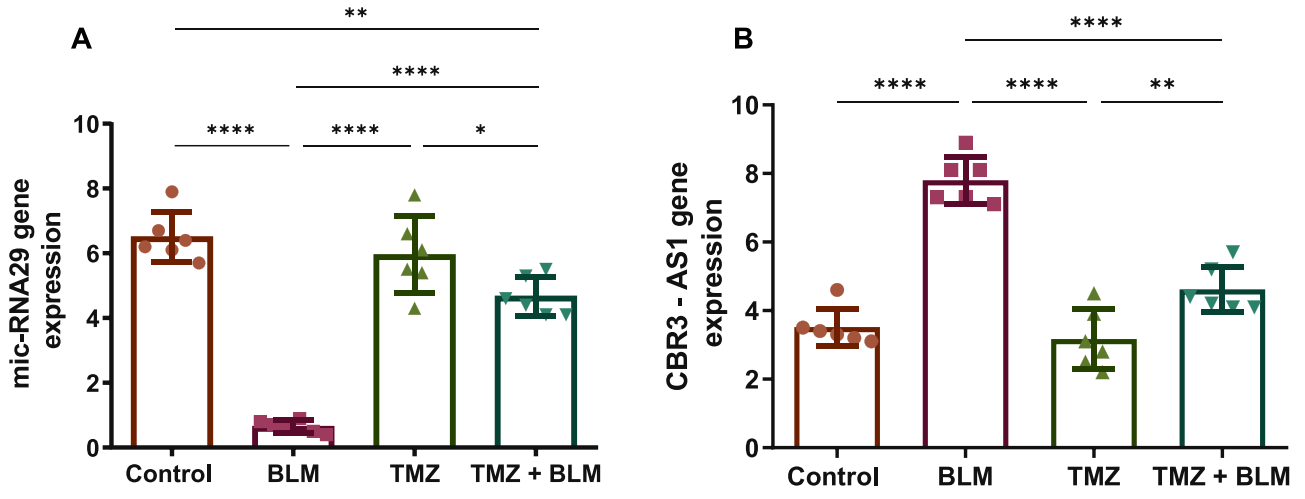

Figure 2 Effect of trimetazidine treatment (15 mg/kg/day; for four weeks) on the expression levels of epigenetic regulator Lnc CBR3-AS1 (**A**), and miRNA-29 (**B**) in BLM-induced lung fibrosis. The data is expressed as mean±SD, with a sample size of n=7. Multiple comparisons were analyzed by one-way ANOVA followed by Tukey's multiple comparisons test.

Notes: The differences between groups were considered significant when toward (*$P<0.05$; **$P<0.01$; ***$P<0.0001$).

(P<0.0001) in the expression of lnc CBR3-AS1 gene as compared to the BLM-treated group. These results further emphasize the role of molecular epigenetic regulation of lnc CBR3-AS1 gene expression in lung fibrosis and suggest that TMZ is an antifibrotic drug for the treatment of lung fibrosis by modulating the epigenetic regulation of lnc CBR3-AS1. To identify the target miRNA of the master regulator lnc CBR3-AS1, we assessed the expression levels of miRNA-29 and explored its role in lung fibrosis. Despite the expression of both miRNA-29 and lnc CBR3-AS1 in lung tissues, the interplay between these genes in lung fibrosis remains poorly understood. In this regard, we evaluated the expression of miRNA-29 in lung tissue after BLM treatment and compared it to that in the control group. As indicated in Figure 2, our findings revealed the BLM administration significantly (P<0.0001) reduced miRNA-29 expression compared to that in the control group. These findings are in agreement with previous reports of reduced expression levels of miRNA-29 in individuals with IPF.[21] These results further suggest the exploration of miRNA-29-based treatments as a potential therapeutic approach for lung fibrosis. In contrast, TMZ treatment showed no considerable effect on the expression of miRNA-29 in the TMZ-treated control group, as compared to the control group. However, there was a substantial reduction (P<0.0001) in the expression levels of miRNA-29 compared with those in the BLM-induced lung fibrosis group. These results suggest that lnc CBR3-AS1 is an epigenetic regulator of miRNA-29, and that both genes play crucial roles in modulating the molecular cascade of lung fibrosis. Furthermore, our findings highlighted the possible therapeutic potential of TMZ in lung fibrosis by targeting epigenetic regulators.

TMZ Significantly Attenuated the Expression of Inflammatory Biomarkers Jagged1 and Notch by Targeting FIZZ-1 in BLM-Induced Lung Fibrosis

FIZZ1 promotes the transformation of lung fibroblasts into myofibroblasts through the activation of the Notch signaling pathway, which is a significant characteristic of lung fibrosis. FIZZ1 also elevated the levels of the activated intracellular domain of Notch1 and its ligand Jagged1, which is linked to increased expression of α-smooth muscle actin (α-SMA) in lung fibrosis. Toward this end, we next focused on assessing the expression of FIZZ1 in lung tissues and explored its interplay with the inflammatory signaling cascade. As shown in Figure 3, the administration of BLM resulted in a notable

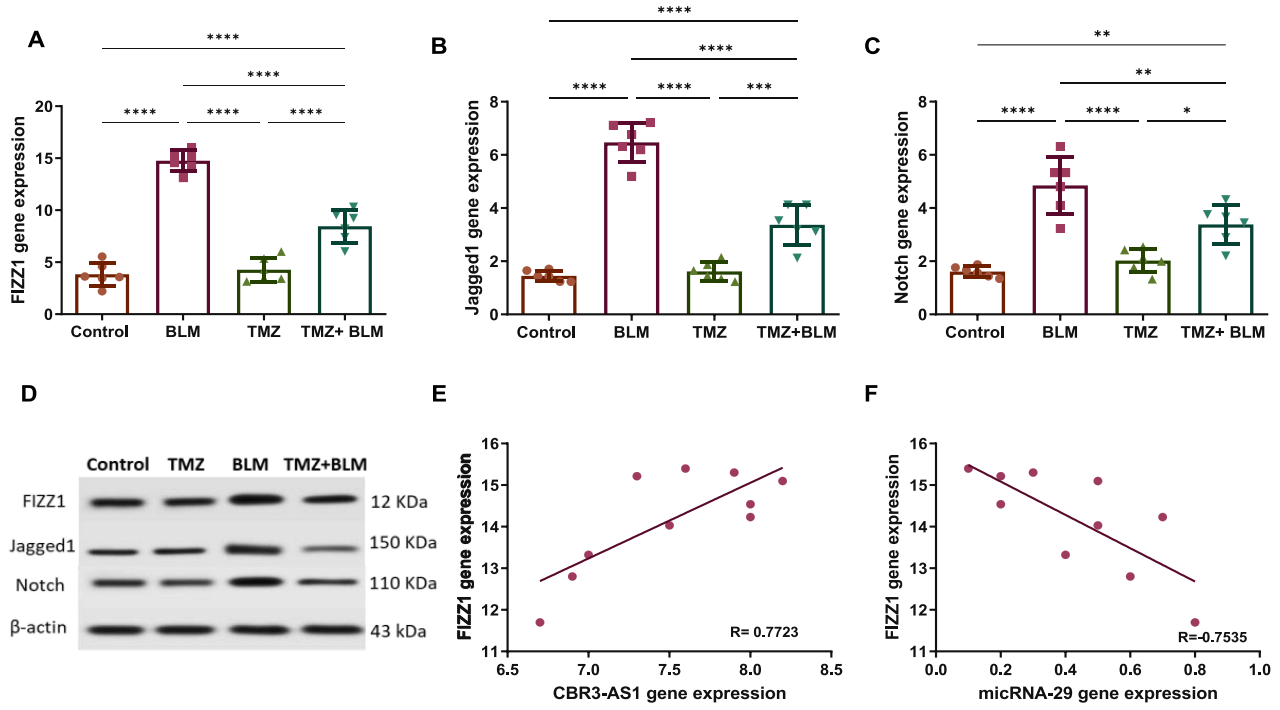

Figure 3 Effect of trimetazidine treatment (15 mg/kg/day; for four weeks) on FIZZ1 (**A**), Jagged1 (**B**) and Notch (**C**) genes and proteins (**D**) expression in BLM-induced lung fibrosis. The correlation study analysis between the expression of tissue FIZZ1 and Lnc CBR3-AS1 (**E**), miRNA-29 (**F**) in BLM-induced lung fibrosis model. The data is expressed as mean±SD, with a sample size of n=7. Multiple comparisons were analyzed by one-way ANOVA followed by Tukey's multiple comparisons test.
Notes: The differences between groups were considered significant when P<0.05 (*P<0.05; **P<0.01; ***P<0.001, ****P<0.0001).

increase ($P<0.0001$) in the expression of FIZZ1 compared to the control group. In agreement with previous studies, these findings suggest that BLM administration leads to FIZZ1 upregulation, which subsequently activates inflammatory pathways in lung tissues, thereby contributing to the development of lung fibrosis. Next, we assessed the therapeutic potential of TMZ in lung fibrosis by assessing the expression of FIZZ1 in the TMZ-treated control and TMZ-treated lung fibrosis model groups. Our results revealed that TMZ administration showed no statistical difference in the expression of FIZZ1 in the TMZ-treated control group compared to that in the control group. Conversely, the TMZ-treated model group exhibited a significant reduction ($P<0.0001$) in FIZZ1 expression compared to the BLM-induced lung fibrosis group. These findings indicated that the antifibrogenic potential of TMZ may be associated with its ability to modulate inflammatory cascades in lung tissues by targeting FIZZ1.

To examine the possible correlation between lnc CBR3-AS1/miRNA-29 and FIZZ1, we performed correlation analysis using Pearson's correlation coefficient between the expression of lnc CBR3-AS1/miRNA-29 and FIZZ1. According to the findings (Figure 3), statistical analysis conducted using Pearson's correlation coefficient indicated a significant ($p<0.05$) positive association between tissue FIZZ 1 and lnc CBR3-AS1 expression (R= 0.7723). Furthermore, our analysis showed a significant negative association between miRNA-29 and FIZZ1 expression (R=−0.7535). Taken together, these results indicate that lnc CBR3-AS1 could be an epigenetic regulator of FIZZ1, and further suggest a possible correlation between miRNA-29 and lncRNA CBR3-AS1 gene expression and FIZZ1-mediated inflammatory pathways in lung fibrosis.

To explore the inflammatory markers associated with FIZZ1, we conducted computational networking analysis using the STRING database to assess the protein-protein association interaction network between FIZZ1 (Retnla) and the inflammatory markers. As shown in Figure S2, the results indicated significant (PPI enrichment with a p-value of $9.41e^{-07}$) interactions between FIZZ1, and the inflammatory markers NOTCH, Jagged (Jag1), Smad3, TGFB, and RelA (NF-kB) (Table S1). The Jagged1/Notch pathway plays a significant role in regulating epithelial-to-mesenchymal transition and myofibroblast formation, a process initiated by FIZZ-1 in alveolar epithelial cells, as part of the progression of chronic lung fibrosis. To gain more insight into the association between FIZZ1 and the Jagged1/Notch inflammatory pathways in BLM-induced lung fibrosis, we assessed the expression levels of Jagged1 and Notch genes. As depicted in Figure 3, our analysis revealed that the administration of BLM significantly upregulated ($P<0.0001$) the expression levels of Jagged1 and Notch genes compared to the control group. These results are in agreement with the previously observed increase in FIZZ1 expression in the BLM-treated model group and indicate the successful induction of fibrosis in lung tissues. Assessment of the therapeutic potential of TMZ revealed that administration of TMZ did not significantly affect the expression of Jagged1 and Notch genes in the TMZ-treated control group compared to the control group. Furthermore, treatment of the BLM-induced lung fibrosis model with TMZ demonstrated a substantial reduction in the expression levels of Jagged1 ($P<0.0001$) and Notch ($P<0.01$) genes, as compared to the BLM-treated group. Notch/ Jagged1 genes have been previously recognized as target downstream genes for lncRNA CBR3-AS1. To further underscore our results, we assessed the protein expression of FIZZ1, Jagged1, and Notch proteins in lung tissue across the various treatment groups by conducting Western blot analysis. As shown in Figure S3, the Western blot analysis corroborated our PCR findings across the different groups. The BLM-treated group exhibited, compared to the control group, a significant augmentation in the expression of FIZZ1, Jagged1, and Notch proteins (Figure S3). Conversely, TMZ treatment notably attenuated the expression of examined proteins in the BLM-induced model. Together, our findings suggest a molecular interplay of the lnc CBR3-AS1/miRNA-29/FIZZ1 axis in regulating the Notch/Jagged1 inflammatory pathway and provide novel molecular insights into how these cascades jointly regulate the progression of lung fibrosis. These results further implied that the observed antifibrogenic potency of TMZ could be attributed to its ability to regulate the lncRNA CBR3-AS1/miRNA-29/FIZZ1 axis in lung tissues.

TMZ Significantly Downregulated the Expression of Inflammatory Biomarkers Smad3 and NFKB by Targeting TGF-β in BLM-Induced Lung Fibrosis

As previously stated, our computational network analysis revealed a significant interaction between FIZZ1 and the inflammatory Smad3, TGFB, and RelA (NF-kB) markers (Figure S2 and Table S1). Accordingly, the expression of TGF-

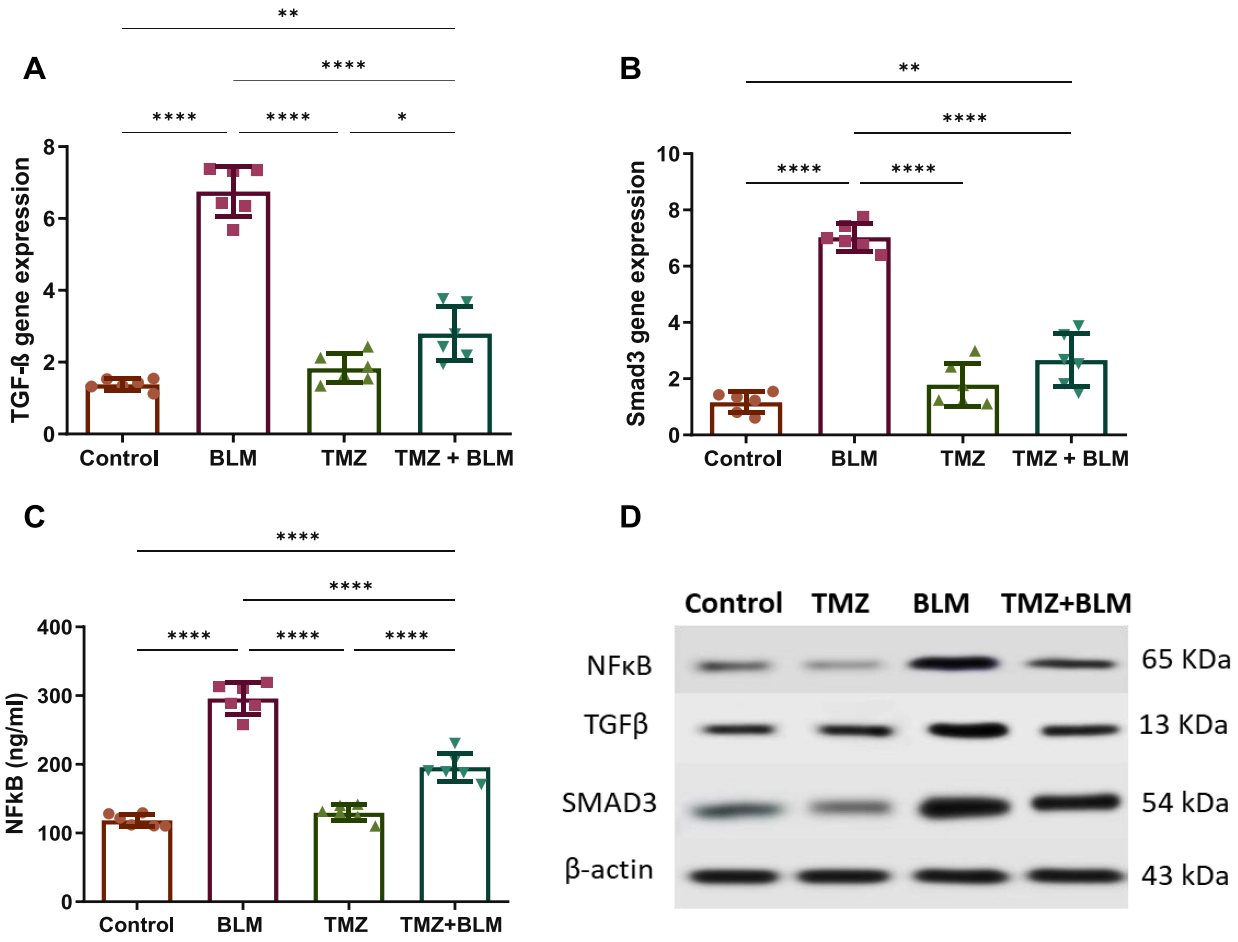

Figure 4 Effect of trimetazidine treatment (15 mg/kg/day; for four weeks) on inflammatory biomarkers TGFB (**A**), Smad3 (**B**), and NFKB (**C**) genes and proteins (**D**) expression in BLM-induced lung fibrosis. The data is expressed as mean±SD, with a sample size of n=7. Multiple comparisons were analyzed by one-way ANOVA followed by Tukey's multiple comparisons test.

Notes: The differences between groups were considered significant when $P<0.05$ (*$P<0.05$; **$P<0.01$; ****$P<0.0001$).

β genes was analyzed to investigate the proinflammatory pathway in lung fibrosis. The TGF-β signaling pathway is associated with fibrosis and inflammation in lung tissues. As presented in Figure 4, BLM administration resulted in a significant increase ($P<0.0001$) in the expression levels of TGF-β compared to the control group. These results indicate that BLM treatment successfully triggered the expression of genes responsible for inflammation and fibrosis in lung tissues. In contrast, treatment of the control group with TMZ showed no considerable difference in TGF-β gene expression, as compared to the control group, while in the BLM-induced lung fibrosis model, there was a significant attenuation ($P<0.0001$) in the expression of the TGF-β gene, as compared to the BLM-treated group. These findings further affirm the therapeutic potential of TMZ in modulating the deteriorating effects of BLM-induced lung fibrosis by targeting the proinflammatory TGF-β pathway. We further explored the inflammatory pathway associated with TGF-β signaling in lung fibrosis by assessing the expression levels of Smad3 and NF-κB. Aligned with TGF-β expression, our findings revealed a significant upregulation ($P<0.0001$) in the expression levels of Smad3 and NF-κB genes in the BLM-treated group compared to the control group (Figure 4). Crosstalk between the Smad3 signaling pathway, driven by the presence of TGF-β, and the activation of NFκB due to lung tissue damage plays a pivotal role in promoting lung fibrosis by orchestrating the production of inflammatory cytokines and fibroblasts within the lung parenchymal tissue. Our results further indicated that BLM treatment induces the inflammatory signaling pathway in lung tissues, resulting in the upregulation of inflammatory cytokines and fibroblasts. Next, we explored the antifibrotic activity of TMZ in lung fibrosis by assessing its ability to target the proinflammatory Smad3 and NF-κB signaling pathways in BLM-induced PF. As depicted in Figure 4, treatment of the BLM-induced PF model with TMZ significantly reduced ($P<0.0001$) the

expression levels of Smad3 and NF-κB genes, as compared to the BLM-treated model. Remarkably, no significant change was observed in the TMZ-treated control group compared with that in the control group. These findings were further validated by conducting Western blot analysis to measure the expression levels of Smad3, NF-κB, and TGF-β proteins in lung tissue across different treatment groups. As illustrated in Figure S4, the Western blot analysis reinforced the PCR results, demonstrating consistency across the different groups. In comparison to the control group, the lung fibrosis model group (BLM-treated group) exhibited a significant increase in the expression of Smad3, NF-κB, and TGF-β proteins, whereas the expression levels were significantly reduced in the TMZ-treated group (Figure S4). The interaction between TGF-β and Smad3/ NFkB triggers the expression of genes responsible for matrix expression, fibroblast differentiation, and proliferation. Furthermore, TGF-β and Smad3 are known as target genes for miRNA-29 and lnc CBR3-AS1, suggesting that the lnc CBR3-AS1/miRNA-29/FIZZ1 axis could be a molecular cascade that modulates inflammatory and fibrotic progression in lung fibrosis. Our findings further indicate that TMZ possesses considerable antifibrotic and anti-inflammatory activities, which are associated with its ability to target the TGF-β, NFκB, and Smad3 signaling pathways in lung fibrosis.

TMZ Modulated the Expression of Oxidative Stress MDA, CAT, SOD and GSH in BML-Induced Lung Fibrosis

An increase in fibroblast growth and myoblast differentiation has been observed under excessive oxidative stress. Previous reports showed that the miRNA-29 and Fizz1 play critical roles in regulating the oxidative stress process in type 2 diabetes Mellitus and pulmonary fibrosis, respectively.[60–64] Accordingly, certain markers of oxidative stress have been identified as valuable in predicting lung fibrosis. To investigate the effect of oxidative stress on the development of lung fibrosis, we assessed the expression of various oxidative stress biomarkers, including malondialdehyde (MDA), catalase (CAT), superoxide dismutase (SOD), and glutathione (GSH). As depicted in Figure 5, the BLM-induced lung fibrosis model exhibited a significant ($P<0.0001$) upregulation in the expression of MDA, coupled with a significant ($P<0.0001$) reduction in serum SOD, CAT, and GSH levels compared to the control group. MDA is a marker of lipid peroxidation, while SOD inhibits oxidative stress. The upregulation of MDA levels following BLM treatment suggested a higher level of oxidative damage in the lungs. SOD and CAT are enzymes that help neutralize harmful reactive oxygen species, whereas GSH is an essential antioxidant. The observed downregulation of serum SOD, CAT, and GSH levels implies a reduction in antioxidant defense mechanisms to counteract oxidative stress. Together, these findings reveal that BLM exacerbates oxidative stress and weakens the capacity of the lungs to defend against it, which may be relevant to the development and progression of lung fibrosis. We further assessed the antifibrotic potential of TMZ by assessing its ability to modulate oxidative stress in BLM-induced lung fibrosis. As shown in Figure 5, in the TMZ-treated control group, TMZ treatment demonstrated no significant effect on the serum expression of MDA, CAT, SOD, and GSH levels, as compared to the control group. Nevertheless, TMZ administration showed the ability to significantly attenuate ($P<0.0001$) the expression levels of MDA, as well as significantly upregulate the expression levels of SOD ($P<0.0001$), CAT ($P<0.0001$) and GSH ($P<0.01$) in BLM-treated model group. Additionally, Western blot analysis was utilized to quantify the expression of oxidative stress proteins in lung tissue across different treatment groups, as depicted in Figure 5. The lung fibrosis model group exhibited, compared to the control group, a significant elevation in the MDA protein expression, while the expression levels of SOD, CAT, and GSH proteins were substantially attenuated. On the other hand, following the TMZ administration, these alterations were reversed. As compared to the BLM-induced PF model, the expression of SOD, CAT, and GSH proteins was significantly augmented, along with significant mitigation in the expression of MAD protein (Figure S5). These findings further affirm the therapeutic potential of TMZ as an antifibrotic drug by reducing the expression of markers that oppose oxidative stress while increasing the expression of markers that activate antioxidant defense mechanisms, ultimately countering oxidative stress.

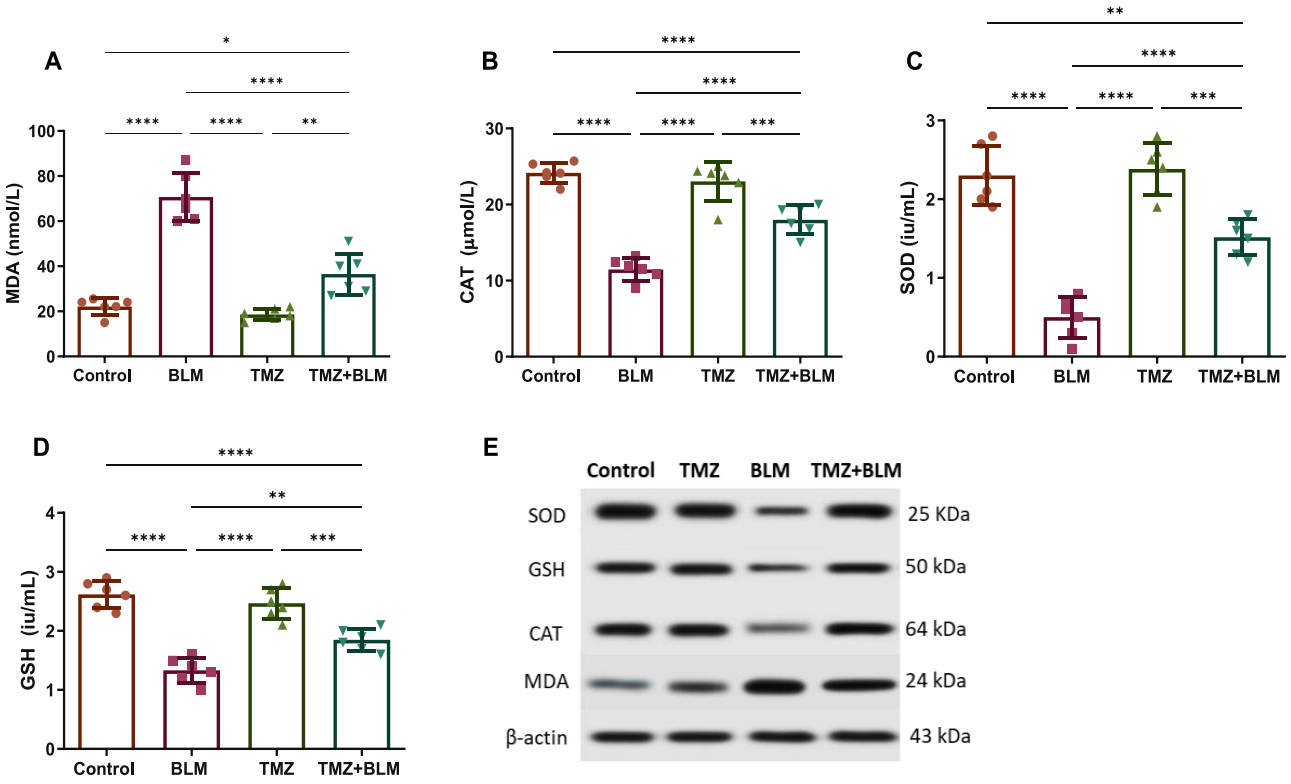

Figure 5 Effect of trimetazidine treatment (15 mg/kg/day; for four weeks) on serum oxidative stress markers MDA (**A**), CAT (**B**), SOD (**C**), and GSH (**D**), and their protein expression by Western blot analysis (**E**) in BLM-induced lung fibrosis. The data is expressed as mean±SD, with a sample size of n=7. Multiple comparisons were analyzed by one-way ANOVA followed by Tukey's multiple comparisons test.

Notes: The differences between groups were considered significant when $P<0.05$ (*$P<0.05$; **$P<0.01$; ***$P<0.001$, ****$P<0.0001$).

TMZ Significantly Reduced the Expression Levels of Serum Immunological Biomarkers ICAM-I and IL-18 in BLM-Induced Lung Fibrosis

Next, we employed computational networking analysis to explore the protein-protein association interaction network between FIZZ1 (Retnla), and immunomodulatory markers. Our findings revealed a significant PPI enrichment (p-value of $2.87e^{-07}$) with interacting nodes linked to the functional protein partners, including ICAM1, IL18, and FIZZ1 (RetLna) (Figure S2 and Table S2). ICAM-1 and IL-18 are well-known immunological chemokines associated with pulmonary inflammation and have garnered attention as promising diagnostic and/or prognostic biomarkers for IPF. The over-expression of ICAM-1 on the surface of endothelial cells plays a significant role in inducing the inflammatory signaling pathway in lung fibrosis. To gain further insight into the immune response in lung fibrosis, we assessed the expression levels of various immunological markers including ICAM-1 and IL-18. As presented in Figure 6, the BLM-treated group demonstrated a significant elevation ($P<0.0001$) in the expression levels of the immunological markers ICAM-1 and IL-18 compared with the control group. These markers are associated with inflammation and immune responses in the lungs, and their elevated expression suggests a heightened immune and inflammatory response. Consistent with previous findings, our results suggest that these markers may play a role in the pathophysiology of lung fibrosis, making them potential targets for further research into the development of potential therapies. To further explore the immunomodulatory function of TMZ, we assessed the expression of ICAM-1 and IL-18 markers in TMZ-treated control and BLM-treated model groups after treatment with TMZ. Our investigations revealed that TMZ treatment had no significant effect on the expression of immunological markers in the TMZ-treated control group compared with the control group. However, there was a significant attenuation ($P<0.0001$) in the expression levels of ICAM-1 and IL-18 compared to those in the BLM-induced lung fibrosis group (Figure 6). These findings were further affirmed by Western blot analysis to evaluate the expression of ICAM-1 and IL-18 proteins in lung tissue across different treatment groups. Our results, aligned with PCR analysis, revealed that the lung fibrosis model group displayed a significant elevation in ICAM-1 and

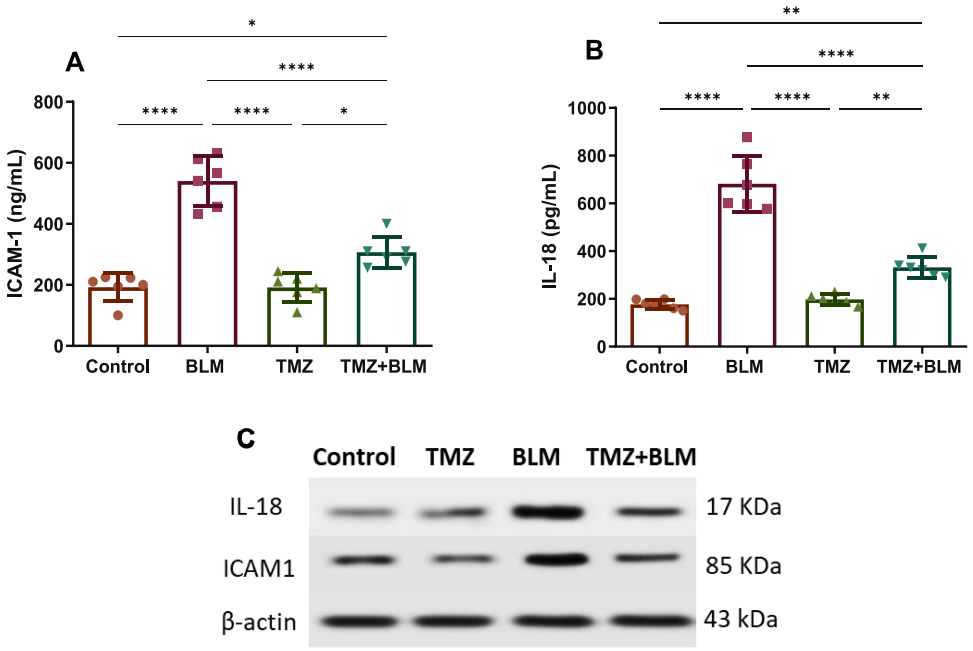

Figure 6 Effect of trimetazidine treatment (15 mg/kg/day; for four weeks) on immunological biomarker ICAM-1 (**A**), IL18 (**B**) and their protein expression by Western blot analysis (**C**) in BLM-induced lung fibrosis. The data is expressed as mean±SD, with a sample size of n=7. Multiple comparisons were analyzed by one-way ANOVA followed by Tukey's multiple comparisons test.
Notes: The differences between groups were considered significant when $P<0.05$ (*$P<0.05$; **$P<0.01$; ****$P<0.0001$).

IL-18 protein expression compared to the control group (Figure S6). In contrast, the TMZ-treated BLM-induced PF model showed a significant mitigation in the expression of these proteins. These findings provide compelling evidence for the immunomodulatory role of TMZ in lung fibrosis, indicating its potential as a therapeutic agent to mitigate the immune and inflammatory aspects of this condition.

TMZ Modulated the Expression of Various Serum and Tissue Fibrogenic Markers (MMP7, TIMP1, CTGF, Hydroxyproline, and Collagen Content) in BLM-Induced Lung Fibrosis

Finally, we assessed the protein-protein association interaction network between FIZZ1 (Retnla), and fibrotic markers utilizing computational networking analysis. As shown in Figure S2, a significant PPI enrichment (p-value < $1.0e^{-16}$) has been observed between MMP7, TIMP1, CTGF (CNN2), collagen (COL1A1), and FIZZ1 (RetLna) (Table S3). Accordingly, the expression of fibrogenic biomarkers CTGF, MMP7, and TIMP1 associated with the initiation and progression of lung fibrosis have been examined among the experimental groups. As shown in Figure 7, BLM administration resulted in a significant increase ($P<0.0001$) in the expression levels of serum MMP7, TIMP1, and CTGF compared with the control group. The observed upregulation of these fibrogenic markers in the BLM-treated group indicated that BLM treatment successfully induced fibrosis and inflammation in lung tissue. Next, we explored the therapeutic potential of TMZ for modulating fibrogenic markers. Our assessments revealed that the administration of TMZ to the control group had no significant effect on the expression levels of these serum fibrogenic markers compared to the control group (Figure 7A–7C). Conversely, TMZ treatment substantially attenuated ($P<0.0001$) the expression levels of serum MMP7, TIMP1, and CTGF markers compared to those in the BLM-induced lung fibrosis group. To further affirm these findings, we examined the expression of CTGF, MMP7, and TIMP1 proteins in lung tissue across different treatment groups using Western blot analysis. As shown in Figure 7, the results revealed a significant elevation in the protein expression of CTGF, MMP7, and TIMP1 in the BLM-treated group, as compared to the control model. While the TMZ-administrated BLM-induced PF model displayed a substantial attenuation in the expression of these

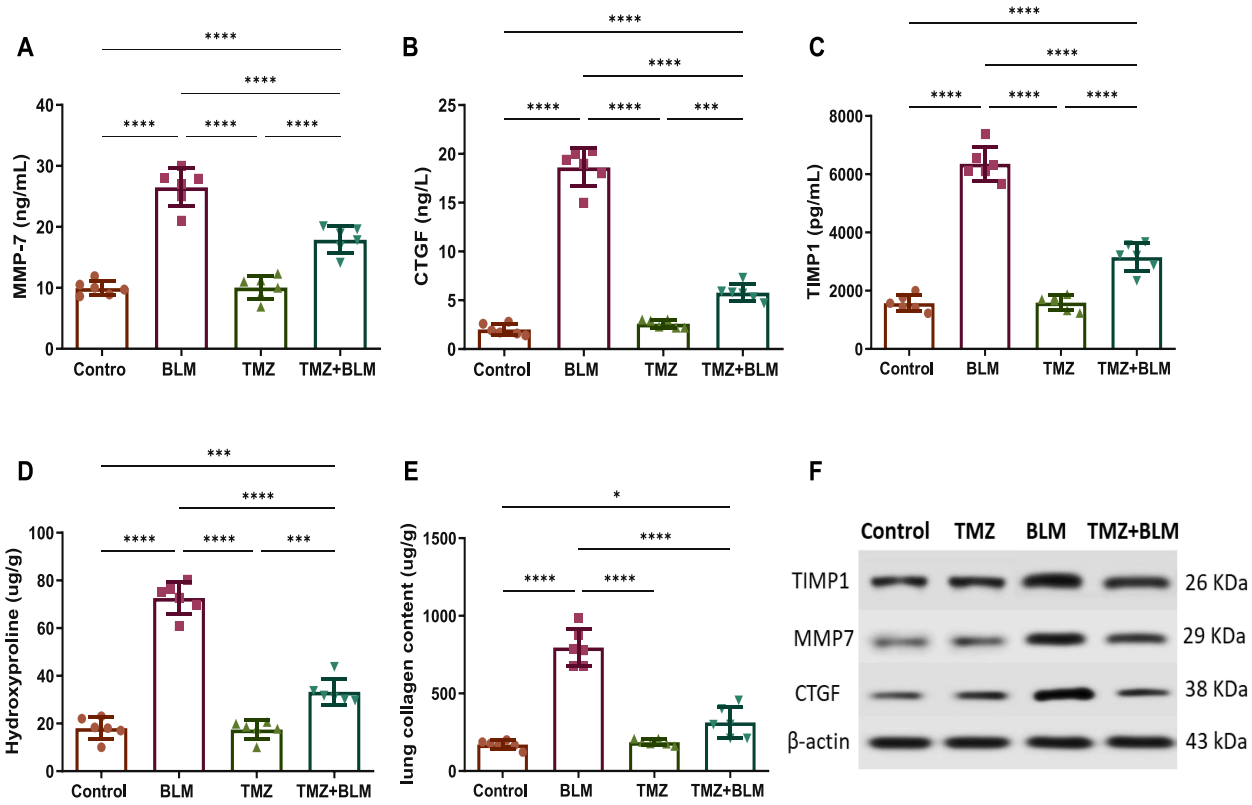

Figure 7 Effect of trimetazidine treatment (15 mg/kg/day; for four weeks) on fibrogenic markers MMP7 (**A**), TIMP1 (**B**), CTGF (**C**), hydroxyproline (**D**), and collagen (**E**), and their protein expression by Western blot analysis (**F**) in BLM-induced lung fibrosis. The data is expressed as mean±SD, with a sample size of n=7. Multiple comparisons were analyzed by one-way ANOVA followed by Tukey's multiple comparisons test.
Notes: The differences between groups were considered significant when $P<0.05$ (*$P<0.05$; **$P<0.01$; ****$P<0.0001$).

proteins (Figure S7). Together, our findings further affirmed the antifibrotic activity of TMZ and its ability to mitigate the detrimental effects of BLM treatment on lung tissues.

We further extended our investigations to assess the expression levels of lung hydroxyproline and collagen. As shown in Figure 7, administration of BLM resulted in a significant elevation ($p<0.0001$) in the expression levels of hydroxyproline and collagen in lung tissue compared to the control group. Elevated expression of hydroxyproline and collagen has been linked to the development of fibrous tissues in the lungs. Next, we explored the therapeutic potential of TMZ in modulating these fibrogenic markers. Our assessments revealed that the administration of TMZ to the control group had no significant effect on the expression levels of lung tissue hydroxyproline and collagen content, as compared to the control group (Figure 7D). Alternatively, TMZ treatment displayed significant mitigation ($p<0.0001$) in the expression levels of hydroxyproline and collagen content in lung tissue compared to the BLM-induced lung fibrosis group. These findings further affirm the antifibrotic potency of TMZ and its ability to reduce lung hydroxyproline and collagen contents, suggesting an effect of TMZ in attenuating the development of fibrosis tissues in the lung.

TMZ Attenuated the Inflammatory Cell Infiltrates and Interalveolar Septum Thickness in BLM-Induced Lung Fibrosis

Analysis of lung sections stained with hematoxylin and eosin (H&E) in the control group revealed the presence of the typical normal architecture of the lung, with thin-walled- alveoli and unobstructed lumina. The alveolar wall comprises of cells with flattened nuclei (pneumocytes Type I), and cubical cells with rounded, bulging nuclei (pneumocytes Type II). A thin interalveolar septum is observed between adjacent alveoli. The average thickness of the interalveolar septa was 7.758 ± 1.256 µm, as indicated by mean values and standard deviations (Figure 8A).

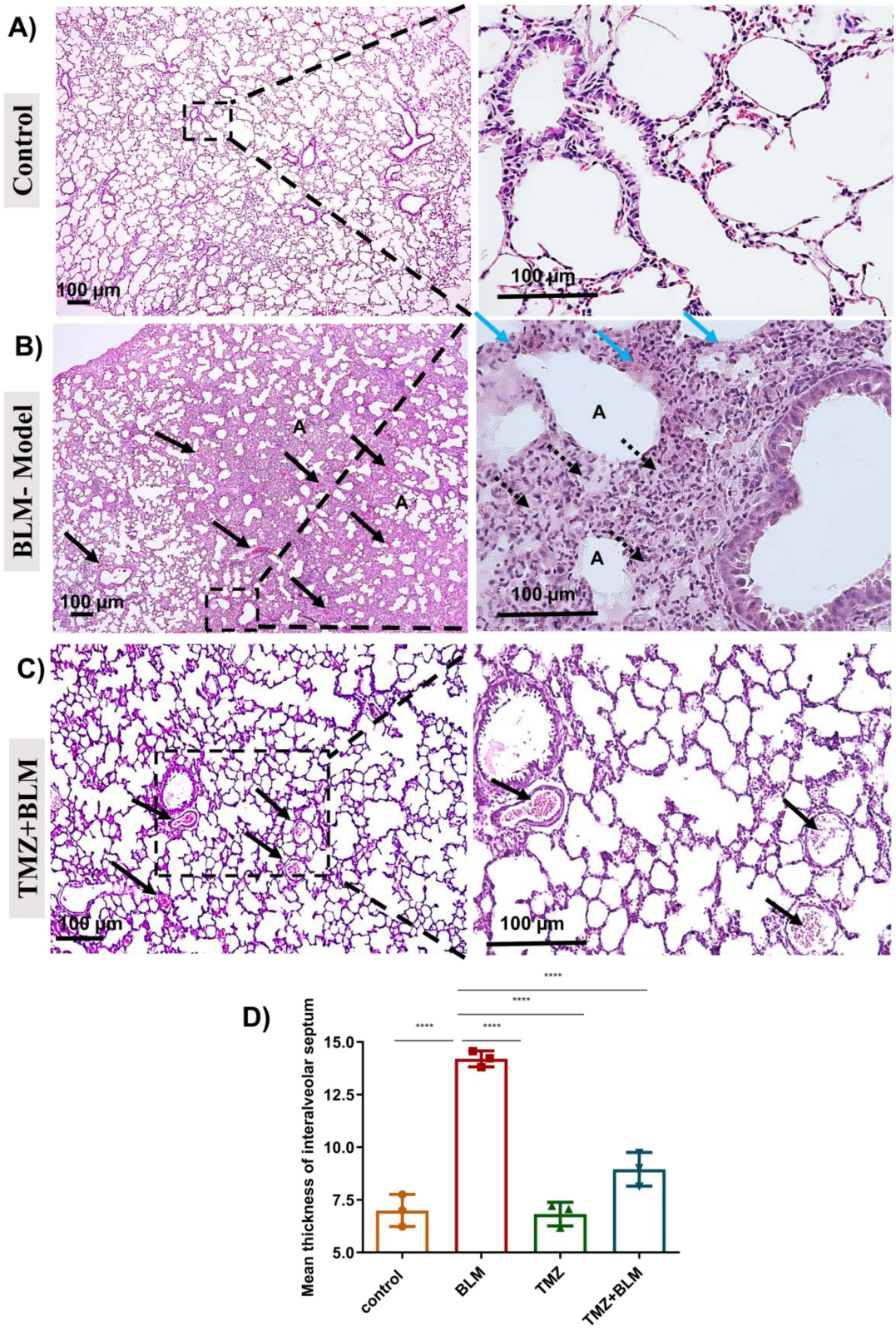

Figure 8 (**A–D**) Photomicrograph of the H&E-stained lung section of the control group (**A**); BLM-Model group (**B**); and TMZ+BLM treated group (**C**). **(A)** The control group shows the normal architecture of the lung, with thin-walled- alveoli and patent lumina. The alveolar wall comprises flat cells with flattened nuclei (pneumocytes Type (I), and cubical cells with rounded, bulging nuclei (pneumocytes Type II). Notice the thin interalveolar septa. (**B**): The BLM-model group shows marked distortion of the lung architecture with the replacement of the lung tissue with collagen fibers (arrowheads), and most of the alveoli collapsed (**A**). Notice markedly thickened interalveolar septa (blue arrows) and numerous congested blood vessels were observed (black arrows). (**C**) The TMZ+BLM treated group shows restoration of the normal lung architectures with numerous alveoli having thin walls and patent lumina. However, numerous blood vessels were congested with erythrocytes (arrows). (**D**): The mean thickness of interalveolar septum ±SD (in µm) in different groups (n=3).

Examination of lung sections from rats subjected to the BLM paradigm revealed significant alterations in the structural organization of the lungs. An obvious distortion of the lung architecture was observed with the replacement of the lung tissue with collagen fibers, and most of the alveoli exhibited signs of collapse. Thickness of the alveolar wall and interalveolar septa were detected. The average thickness of the interalveolar septa was 14.565±1.887 µm, as indicated by mean values and standard deviations. Inflammatory cellular infiltration was noted in the interalveolar septa as well as in the vicinity of the bronchioles and blood vessels. Certain regions exhibited significant accumulation of inflammatory cells, predominantly lymphocytes. Furthermore, numerous congested blood vessels were found within the lung parenchyma (Figure 8B).

The TMZ+BLM treated group shows restoration of the normal lung structure with a higher prevalence of alveoli with thin walls than that of the model group. The interalveolar septal thickness was moderate. The average thickness of the interalveolar septa was 9.001±1.167 µm, as measured by mean and standard deviation. However, numerous blood vessels were found to be congested with erythrocytes. No aggregation of inflammatory mononuclear cells was noticed (Figure 8C). Statistical analysis revealed that the mean thickness of the interalveolar septum in the BLM-Model group was significantly greater than that in both the control and TMZ+BLM-treated groups. However, there were no significant differences between the control and TMZ+BLM-treated groups (Figure 8D).

TMZ Mitigated Collagen Fiber Deposition in BLM-Induced Lung Fibrosis

To examine the degree of lung fibrosis, Masson's trichrome staining was performed and the degree of collagen fiber deposition in the lung was compared among the experimental groups. The collagen fibers were observed as elongated and undulating green-colored fibers upon staining. The Masson's trichrome stained lung sections of rats in the control group exhibited normal distribution of tinny few collagen fibers within the pulmonary tissue including the lung parenchyma, interalveolar septa, and the peribronchial and perivascular tissues (Figure 9A). The average ± standard deviation area percentage of collagen fibers was 2.596 ± 0.513.

Analysis of Masson's trichrome-stained lung sections from rats in the BLM-treated model revealed a marked deposition of condensed, thickened collagen fibers in the lung parenchyma with replacement of the normal lung architecture and distortion of the majority of the alveoli in the vicinity. Furthermore, a significant increase in the quantity of peribronchial and perivascular collagen fiber deposition was detected in comparison to that of the control group. Additionally, several congested blood vessels were observed (Figure 9B). The average area percentage of the collagen fibers was 12.901±1.644.

Analysis of lung sections from rats in the TMZ+BLM-treated group stained with Masson's trichrome revealed a noticeable reduction in the number of collagen fibers compared to the BLM-model group. Few tinny collagen fibers were observed within the interalveolar septa. A slight augmentation in the quantity of collagen fibers was found surrounding the bronchioles and blood vessels in comparison to the model group. However, numerous congested blood vessels were observed as compared to that of the control group. The average area percentage of collagen fibers was calculated as 6.125 ±0.908 (Figure 9C). Statistical analysis demonstrated a substantial increase in the mean area% of collagen fibers ±SD in the BLM-Model group compared to both the control group and the TMZ+BLM treated groups. Furthermore, both cohorts exhibited statistically significant alterations in comparison to one another (Figure 9D).

TMZ Decreased the Percentage of Positive α-SMA Immune Reaction in BLM-Induced Lung Fibrosis

We further extended our investigations to conduct immunohistochemical assessment using α-SMA antibodies. Upon analysis of the lung sections, the positive reaction was observed as dark brown staining. In the control group, a minimal positive immune response was observed in the alveolar lining, interalveolar septa, and blood vessel walls (Figure 10A). The mean ± SD of the positive α-SMA area (%) was 0.740 ± 0.143. The BLM-Model group had a purportedly heightened immune response toward α-SMA antibodies. In contrast to the control group, a discernible dark brown discoloration was observed within the lung parenchyma, interstitial tissue, the interalveolar septa (between the collapsed alveoli), and the peribronchial tissues (Figure 10B). The average percentage area of positive α-SMA immune reactivity was 3.028±0.877,

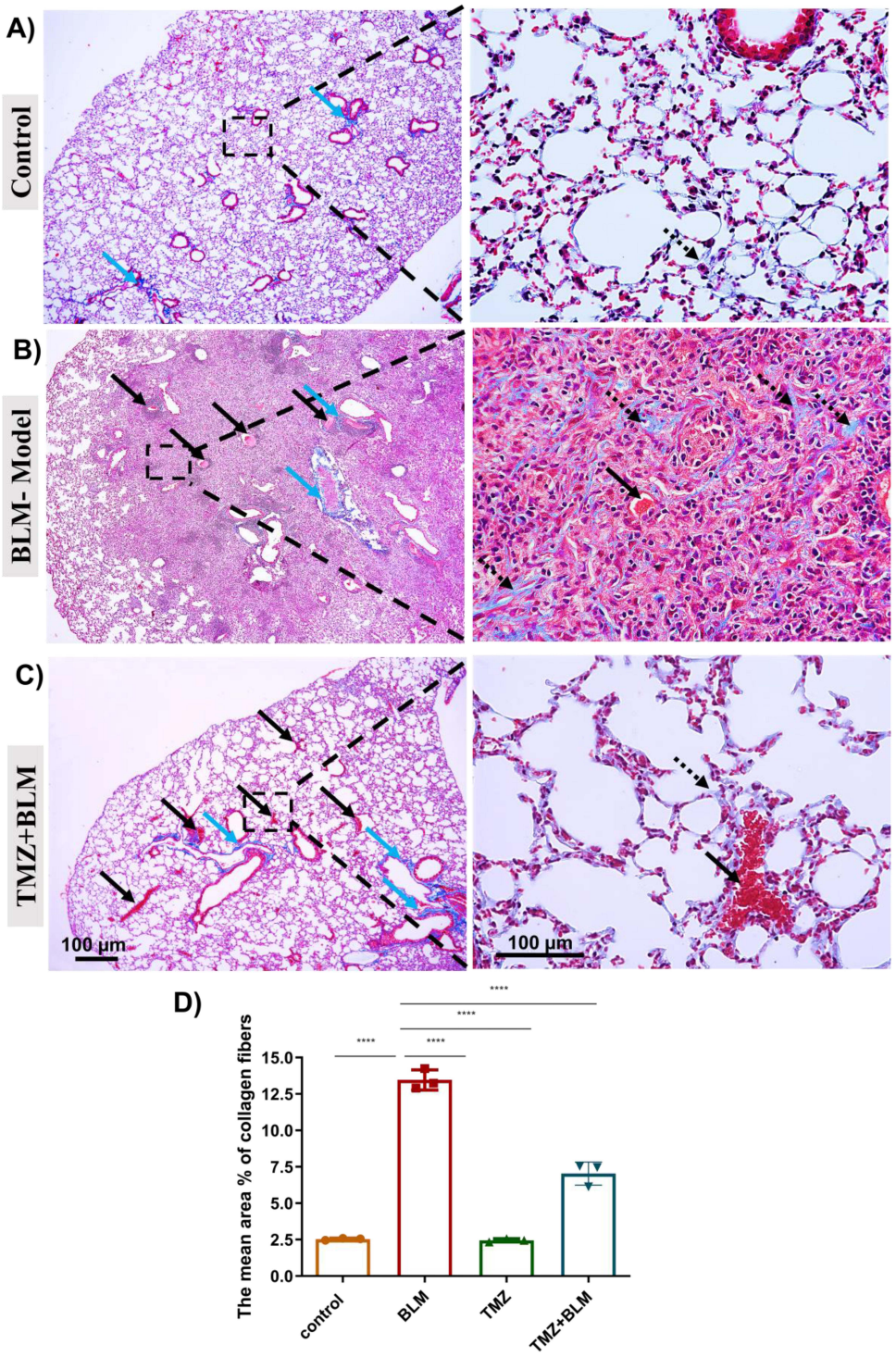

Figure 9 (**A–D**) Photomicrograph of Masson's trichrome-stained lung section of the control group (**A**); BLM-Model group (**B**); and TMZ+BLM treated group (**C**]. (**A**): The control group shows a normal distribution of tinny few collagen fibers in the lung parenchyma and interalveolar septa (dashed arrows), as well as in the peribronchial and perivascular tissues (blue arrows). (**B**) The BLM-model group shows a marked replacement of the lung architecture with the numerous collagen fibers (arrowheads) that distort most of the alveoli in the vicinity (**A**). Notice the apparently higher amount of collagen fibers in the peribronchial and perivascular tissues (blue arrows), and numerous congested blood vessels were observed (black arrows). (**C**) The TMZ+BLM treated group shows restoration of the normal lung architectures with numerous alveoli having thin walls with tinny few collagen fibers in the interalveolar septa (dashed arrows). However, numerous blood vessels were congested with erythrocytes (arrows), and apparently larger amounts of collagen fibers in the peribronchial and perivascular tissues (blue arrows). (**D**): The mean area % of collagen fibers ±SD in different groups with a sample size of n=3. Multiple comparisons were analyzed by one-way ANOVA followed by Tukey's multiple comparisons test.
Note: The differences between groups were considered significant when $p<0.05$ (****$p<0.0001$).

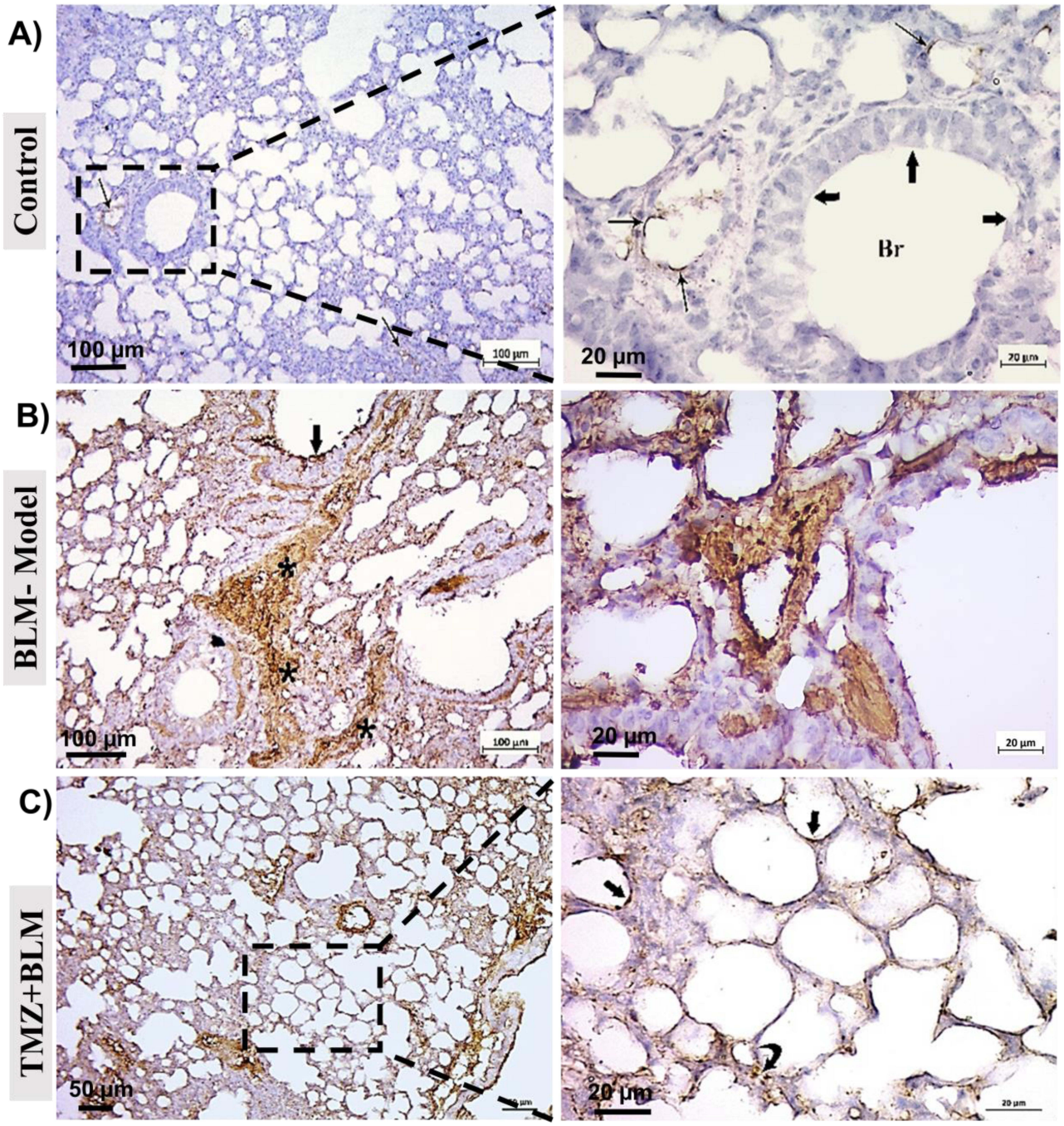

Figure 10 (**A–C**) Photomicrograph of immunohistochemical-stained lung section of the control group (**A**); BLM-Model group (**B**); and TMZ+BLM treated group (**C**) with alpha-smooth muscle actin (α-SMA) antibody. **(A)** The control group shows a thin positive immune reaction to α-SMA antibodies seen as dark brown staining in the cytoplasm of some cells as well as in the interalveolar septa (thin arrows), with intact lining epithelium (thick arrows) of a bronchiole (Br). (**B**) The BLM-model group shows an intense positive immune reaction to α-SMA antibodies in the lung parenchyma (*) as well as in the interalveolar septa (thick arrows). (**C**) The TMZ+BLM treated group shows apparently decreased positive immune reaction to α-SMA antibodies as compared to the BLM-Model group with tinny few positive collagen fibers in the alveolar wall (dashed arrows), and the interalveolar septa (Curved arrow).

as indicated by the mean ±SD. The TMZ+BLM group exhibited a noticeable reduction in positive immunological responses to α-SMA antibodies in the walls of the alveoli, the interalveolar septa as well as around a few bronchioles compared to the BLM-model group (Figure 10C). The average ± SD area percentage of the positive α-SMA immune reaction was 1.23± 0.355.

Statistical analysis demonstrated a substantial increase in the mean area% of positive α-SMA immune reaction ±SD in the BLM-Model group compared to both the control group and the TMZ+BLM group. However, no significant differences were observed between the groups when comparing their changes (Figure 11). To affirm our results, Western blot analysis was executed to measure the expression of α-SMA in lung tissue of different treated groups, as shown in Figure 11. The analysis reinforced our histological results in the different groups. Compared to the control group, the lung fibrosis model group showed significant elevation in the expression of α-SMA while expression was significantly reduced in the TMZ-treated group.

Discussion

The World Health Organization (WHO) has identified cardiovascular, pulmonary, and newborn diseases as significant factors that contribute to global mortality.[65] Pulmonary fibrosis is characterized by abnormal activation and transformation of lung fibroblasts, prolonged damage to the alveoli, and overproduction of the ECM.[66] To date, the treatment of lung fibrosis is limited and primarily aimed at symptom management and slowing disease progression, rather than providing a cure. In the current study, we demonstrated the protective effect of TMZ in attenuating BLM-induced lung fibrosis for the first time. BLM has traditionally been employed in rat models to induce lung fibrosis, enabling the investigation of fibrogenic mechanisms and evaluation of prospective therapeutic interventions. BLM induces DNA strand breaks, which triggers inflammation and lung damage, leading to interstitial fibrosis.[67] Fibrosis is characterized by inflammation, cell infiltration, epithelial damage, ECM build-up, septa thickening, scarring, fibroblastic foci, and architectural changes in the lung tissue.[68] While long non-coding RNAs, including lncRNA CBR3-AS1, have garnered attention for their roles in diverse diseases, including cancer, their role in lung fibrosis remains unclear. We envisioned uncovering how this intricate molecular cascade collectively regulates the initiation and progression of lung fibrosis. Furthermore, we explored the pharmacological potential of TMZ in attenuating lung fibrosis by targeting the identified LncRNA CBR3-AS1/miRNA-29/FIZZ1 axis. Our study ventured into this unexplored domain by examining the potential

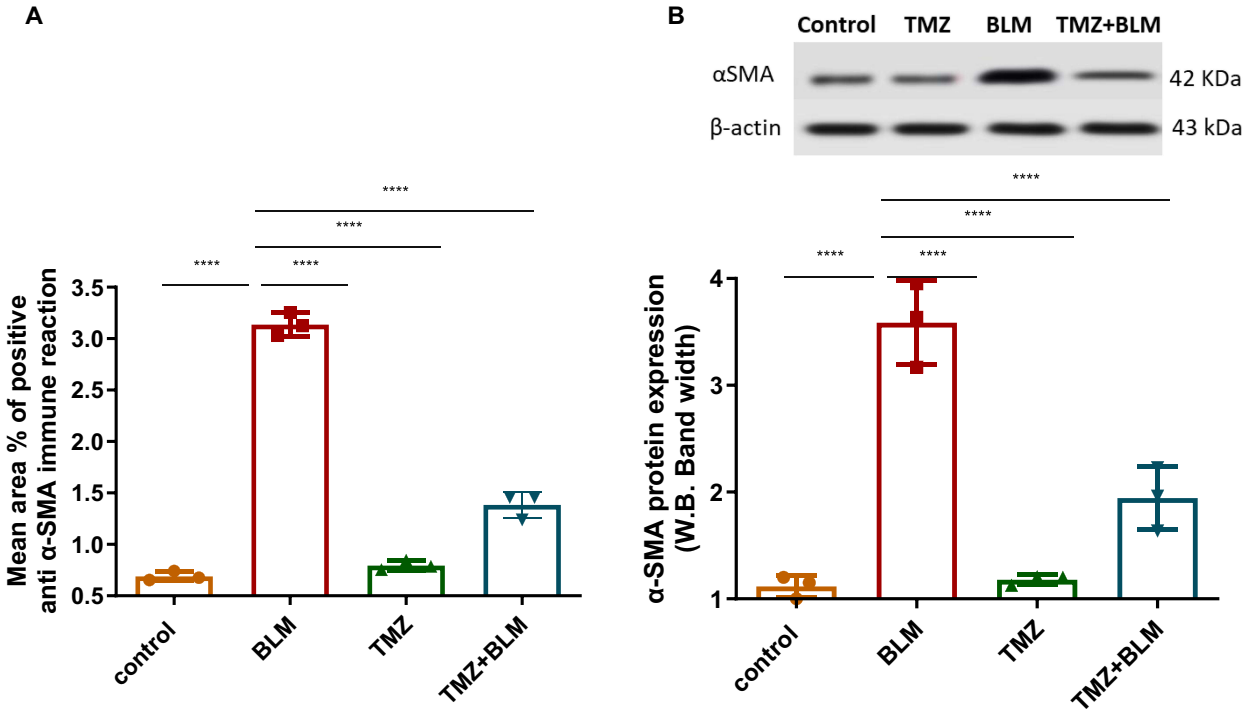

Figure 11 (**A**) The mean area % of positive anti-α-SMA immune-reaction ±SD in different groups. (**B**) Western blot analysis for the expression of α-SMA in the experimental groups. The data is expressed as mean±SD, with a sample size of n=3. Multiple comparisons were analyzed by one-way ANOVA followed by Tukey's multiple comparisons test.

Note: The differences between groups were considered significant when $p<0.05$ (****$p<0.0001$).

contributions of Lnc CBR3-AS1 in orchestrating fibrosis-related pathways in the lung. Similarly, while previous research has demonstrated the significance of miRNA-29 in regulating gene networks and fibrotic processes, our study aimed to unravel its specific involvement within the context of lung fibrosis. The unique aspect of our study lies in bridging the molecular mechanisms by which miRNA-29 and Lnc CBR3-AS1 might influence the development of lung fibrosis. Our findings revealed that lncRNA CBR3-AS1 was upregulated in response to BLM treatment, implying its role in promoting lung fibrosis. Simultaneously, miRNA-29 expression was significantly decreased in BLM-induced lung fibrosis, consistent with its known targets, including Notch, Jagged1, and TGFβ1, which play crucial roles in promoting epithelial-mesenchymal transition. These findings underscore the notion that Lnc CBR3-AS1 and miRNA- 29 may act as epigenetic regulators of lung fibrosis development (Figure 12). Our observations are consistent with those of a previous study that also identified Lnc CBR3-AS1 as a versatile player in enhancing radiosensitivity in NSCLC. The study highlighted that Lnc CBR3-AS1 acts as a competing endogenous RNA for miRNA-509-3p and unveiled regulatory networks involving downstream targets, such as histone deacetylase 9.[16] Additionally, our findings resonate with those of another study that demonstrated the antifibrotic effect of miRNA-29 via modulation of the fibrotic TGF-β1/Smad signaling pathway.[69] Furthermore, Zhao et al recently reported that lncRNA CBR3-AS1 can directly interact with microRNA-29a leading to the inhibition of miRNA-29a-mediated cell migration and invasion.[19] These findings indicate that lncRNA CBR3-AS1and miRNA-29 are key regulatory players in Notch/Jagged1/Smad3/TGF-ß1 signaling events. However, it is noteworthy that the present study represents the first attempt to explore the potential correlation between the Lnc CBR3-AS1/miRNA-29/FIZZ1 axis and modulation of the Notch/Jagged1/Smad3/TGF-ß1 signaling pathway. Our findings revealed significant upregulation of FIZZ1 expression in response to the BLM-induced model, suggesting that Fizz1

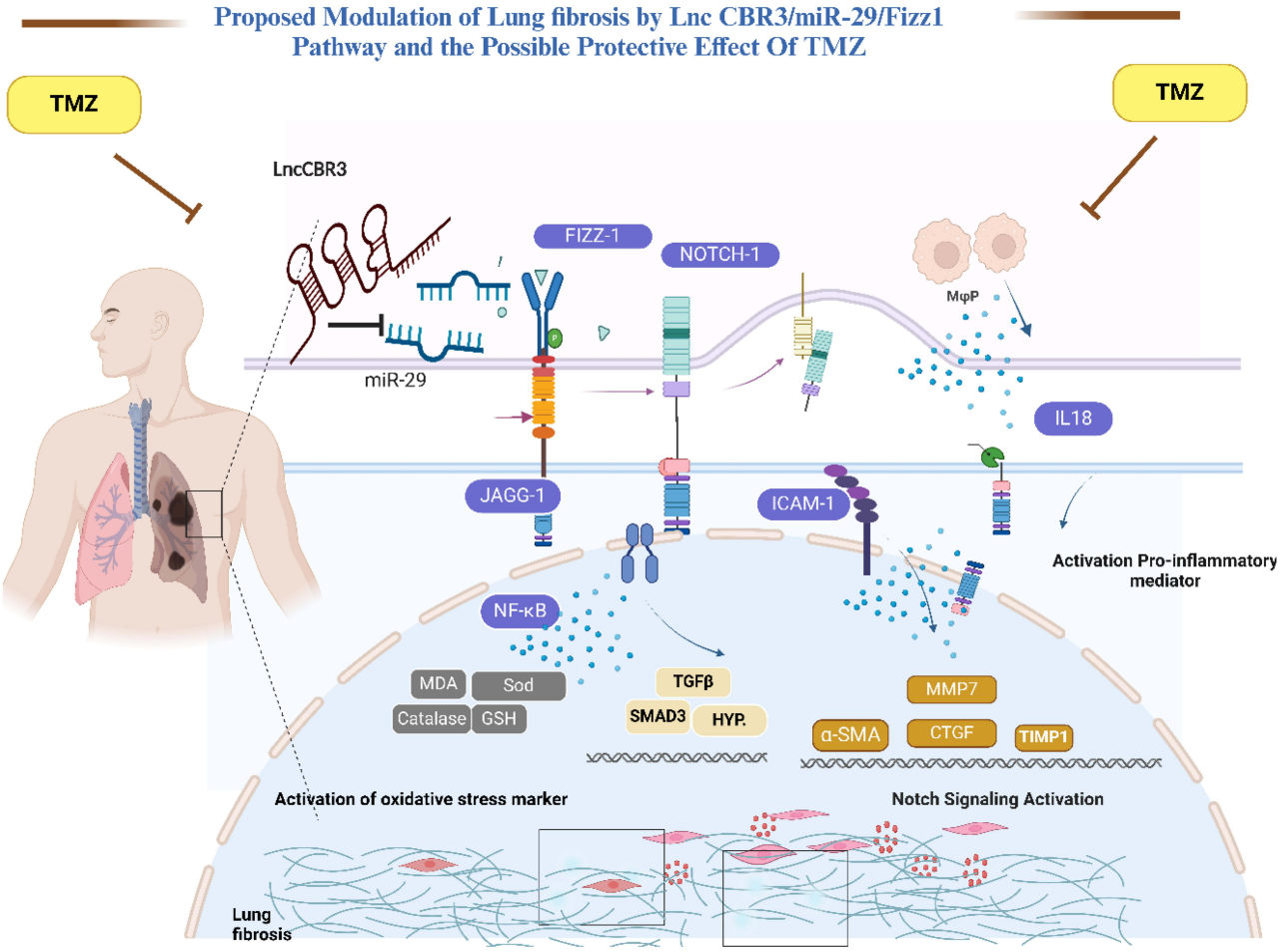

Figure 12 The proposed mode of action for the therapeutical potential of TMZ in BLM-induced lung fibrosis.

could be a downstream target gene for Lnc CBR3 AS1 /miRNA-29 in the context of lung fibrosis (Figure 12). These findings are consistent with those of Liu et al who posited the significance of FIZZ1 in the initiation of BLM-induced PF.[70] Conversely, our study revealed that the use of TMZ substantially reduced the expression of Lnc CBR3-AS1 while elevating the levels of miRNA-29. This suggests that TMZ may hold promise as an antifibrotic treatment. Furthermore, TMZ administration resulted in a notable reduction in FIZZ1 expression, indicating that TMZ has the potential to alleviate the fibrotic effects of BLM on lung tissue by influencing the Lnc CBR3-AS1/miRNA-29/FIZZ1 axis.

Next, we examined the expression pattern of the Notch/Jagged1/Smad3/TGF-ß1 pathway in BLM-induced lung cancer. Our results revealed substantial upregulation of Notch/Jagged1/Smad3/TGF-ß1 genes in BLM-induced pulmonary fibrosis. In agreement with our findings, Yin et al demonstrated the involvement of the Jagged1/Notch1 signaling pathway in the transition of endothelial cells to myofibroblasts in BLM-induced PF rats.[71] Similarly, a previous study showed that TMZ exhibited the ability suppressed extracellular matrix proteins (Colla1 and α-SMA) and blocked the TGFβ/Smad signaling pathway in a liver fibrosis model, ultimately inhibiting liver fibrosis and hepatic stellate cell proliferation.[42] In contrast, the application of TMZ resulted in a remarkable decrease in the expression of these genes in the BLM-treated model. These results indicated that TMZ has the potential to mitigate PF progression by selectively targeting the Notch/Jagged1/Smad3/TGF-ß1 signaling pathway. To further investigate the protective mechanisms of TMZ, our focus shifted toward examining the underlying inflammatory processes that contribute to the development of pulmonary fibrosis, particularly by scrutinizing the NF-κB inflammatory pathway. Our study revealed that BLM treatment significantly activated the NF-κB pathway and stimulated fibroblast production. Conversely, administration of TMZ led to the inhibition of the NF-κB inflammatory pathway in the context of BLM-induced lung fibrosis. These findings align with previous studies that have highlighted the pivotal role of the NF-κB transcription factor in both initiating and advancing fibrotic responses, primarily through its influence on the expression of proinflammatory cytokines such as TNFα, IL6, IL1β, and TGFβ.[72,73] Moreover, Zhang et al demonstrated that TMZ successfully mitigated oxidative stress and apoptosis in cardiomyocytes (Figure 12). This was achieved by activating the Nrf2/HO-1 pathway, while concurrently inhibiting the NF-κB signaling pathway.[74]

Next, we assessed the potency of TMZ to modulate oxidative stress damage in BLM-induced PF. Notably, TMZ effectively decreased the levels of MDA, a marker of oxidative damage, suggesting its potential to reduce oxidative stress in the lung tissues. Furthermore, TMZ treatment increased the expression of SOD, catalase, and GSH, which are essential antioxidant enzymes, suggesting that TMZ plays a crucial role in mitigating oxidative stress in lung fibrosis. Consistent with our findings, TMZ demonstrated the ability to mitigate oxidative stress damage to cardiomyocytes in an exercise-induced myocardial injury model by upregulating SOD and GSH levels and reducing MDA levels.[74] To investigate the immunological activity of TMZ, it is essential to explore its potential impact on the key immunological regulatory factors involved in the immune response to PF, including ICAM-1 and IL-18. Our findings indicate that BLM injection significantly elevated IL-18 and ICAM-1 levels, potentially suggesting the enhanced deposition of fibrous tissue within the pulmonary region. Conversely, the administration significantly attenuated the serum levels of IL-18 and ICAM-1, confirming its potential to inhibit leukocyte migration into inflamed areas and ameliorate pulmonary fibrosis (Figure 12). Elevated IL-8 levels have been observed in the blood of patients with IPF and are associated with a potent chemotactic effect on neutrophils. Furthermore, a negative correlation between IL-18 levels and lung function has been reported in IPF.[75] In our study, BLM injection significantly increased IL-18 levels, potentially indicating an increased deposition of fibrous tissue in the lungs. In contrast, TMZ administration significantly reduced IL-18 concentrations, suggesting its potential role in mitigating lung inflammation and fibrosis. In agreement with our findings, previous studies have shown that ICAM-1 levels increase in the serum and pulmonary epithelial cells of IPF patients.[76,77]

We further explored the potential of TMZ to suppress inflammatory regulators in BLM-induced lung fibrosis by examining the expression levels of the relevant fibrogenic components, including MMP7, CTGF, TIMP-1, and lung hydroxyproline. Our findings revealed that TMZ possesses antifibrotic properties in BLM-induced lung fibrosis through a reduction in MMP-7 levels, which plays a crucial role in the degradation and restructuring of various components within the ECM.[78] These results align with a study that reported elevated MMP-7 levels in patients with IPF compared to healthy controls, suggesting that MMP-7 is a reliable predictor of lung function and disease progression.[79] Furthermore, our findings suggest that TMZ has the potential to reduce the level of CTGF in BLM-induced lung fibrosis, indicating the

effect of TMZ on collagen synthesis.[80] Furthermore, our results indicate that TMZ administration significantly decreased CTGF levels in the BLM-induced model, confirming its antifibrogenic role. Consistent with our findings, a previous study indicated that TMZ effectively decreased the expression of CTGF protein in both myocardial tissue and myocardial fibroblasts in diabetic rats, suggesting that TMZ has the potential to reduce collagen production in myocardial fibroblasts, ultimately leading to an antifibrotic effect.[81] To gain insights into the antifibrogenic role of TMZ, we delved into a crucial fibrogenic marker in IPF, TIMP-1. Our study revealed a substantial increase in TIMP-1 levels following BLM administration, indicating increased fibrous tissue deposition in the pulmonary region. However, TMZ administration significantly reduced TIMP-1 levels (Figure 12). In support of our findings, Manoury et al reported early dysregulation of TIMP-1 following BLM treatment, suggesting its involvement in the development of pulmonary fibrosis.[82] These results further underscore the promising antifibrogenic effects of TMZ in countering fibrotic processes by targeting TIMP-1. We further examined the effect of TMZ on hydroxyproline levels in the lung tissue, a common indicator of fibrosis severity in BLM-induced lung fibrosis. BLM treatment significantly increased lung tissue hydroxyproline levels, indicating an increased deposition of fibrous tissue in the lungs. However, TMZ administration significantly reduced hydroxyproline levels in the lung tissue. This suggests that TMZ effectively reduced fibrous tissue accumulation, collagen synthesis, and fibrotic progression in the lungs, supporting its therapeutic potential in PF. Consistent with our findings, Yukselen et al affirmed that the application of TMZ to esophageal caustic injury rat models resulted in substantial improvements in histopathological damage concomitant with a noticeable decrease in tissue hydroxyproline content.[83]

Our study provides evidence supporting the anti-inflammatory and antifibrotic properties of TMZ in mitigating structural damage in BLM-induced PF. To confirm our findings, we performed detailed histological and morphometric analysis. In our study, we observed the characteristic histological features of lung fibrosis in the BLM-model group: collapsed, uneven, and thicker walls with thick interalveolar septa. Bronchiole linings showed irregularities, such as thickening, detached epithelial cells, and luminal inflammation. The BLM-induced PF group treated with TMZ showed a significant improvement in the structural integrity of the lungs, including open passageway alveoli and thin membranes, compared to the BLM-model group. The percentage area of collagen fibers exhibited a considerable drop in comparison with the control group; however, it remained significantly greater than that of the control group. Furthermore, the BLM-induced PF group treated with TMZ exhibited a reduction in positive immune responses to α-SMA antibodies within the bronchiole and blood vessel walls, as well as in the interalveolar septa, compared with the BLM-model group. Morphometric analysis revealed significantly thicker interalveolar septa and increased collagen in the septa, near bronchioles, and blood vessels in the BLM model group, leading to proinflammatory and profibrotic molecule production. Pneumocyte type II activation and fibroblast proliferation subsequently increases collagen deposition, thickening of the septum, and alveolar collapse.[84] Our investigation aligns with previous research; we identified inflammatory cellular infiltrates in the lung tissue, including the interalveolar septa, around the bronchioles, and blood vessels.[85] Our investigations have also identified pronounced swelling and vacuolation of the alveolar cells.[86] Researchers have reported the presence of type I pneumocyte hydropic degeneration in inflammatory cells upon BLM administration, which was attributed to its cytotoxic effect.[87] We also employed immunohistochemical techniques to determine the presence of α-SMA in the lung tissue across various experimental groups. The presence of a dark brown stain in the cytoplasm of cells located in the blood vessel wall (smooth muscle) and bronchial wall (myofibroblasts) indicated a favorable immunological response to α-SMA.[88] Myofibroblasts are contractile cells that originate from activated fibroblasts and play a significant role in fibrosis.[89] Notably, the presence of α-SMA-positive cells is indicative of EMT. During EMT, epithelial cells undergo transformation, lose their polarity, break cell junctions, and assume an elongated mesenchymal-like shape. They also express mesenchymal markers, such as fibronectin and α-SMA, which ultimately lead to increased deposition of collagen.[90] The current study revealed the presence of cells expressing α-SMA in the epithelial lining of the bronchioles and alveoli in the BLM model group. Furthermore, this group demonstrated a statistically significant increase in the percentage of α-SMA immunoreactivity within the area.

Conclusion

In the present study, we provide evidence for a new molecular interplay axis for lung fibrosis (lncRNA CBR3-AS1/miRNA-29/FIZZ1) and its association with inflammatory pathways, oxidative stress, and immunological responses in

lung fibrosis. Our results revealed that BLM treatment significantly upregulated the expression of lncRNA CBR3-AS1 and FIZZ1, along with the downregulation of its competing endogenous miRNA-29. Our study revealed that FIZZ1 gene expression could be regulated by the lncRNA CBR3-AS1/ miRNA-29, and that these genes could be potential early diagnostic markers for lung fibrosis and targeted therapy. The novelty of our study lies in identifying and elucidating the previously unexplored lncRNA CBR3-AS1/miRNA-29/FIZZ1 axis, demonstrating its critical role in regulating lung fibrosis. This connection offers a deeper understanding of the underlying mechanisms involved in lung fibrosis and provides a potential target for future therapeutic interventions. Notably, our study reveals the potential therapeutic value of TMZ in mitigating lung fibrosis. By targeting the lncRNA CBR3-AS1/miRNA-29/FIZZ1 axis, TMZ mitigated the negative effects of bleomycin through the reduction of oxidative stress, inflammation, and the levels of immunological and fibrogenic markers. This suggests that TMZ holds promise as an antifibrotic drug, providing new avenues for the treatment of pulmonary fibrosis. In summary, our study enhances our knowledge of the molecular mechanisms contributing to lung fibrosis and highlights the potential of TMZ as a promising therapeutic option. Further research and clinical studies are necessary to validate our findings and to establish the long-term safety and efficacy of TMZ as a potential therapeutic approach for individuals with PF.

Data Sharing Statement

Data supporting the results reported in this manuscript are included in this article. The raw data supporting the conclusions of this article will be made available by the corresponding authors without any undue reservation.

Institutional Review Board Statement

The animal study protocol was performed following the local legislation and institutional requirements and approved by the Institutional Review Board (or Ethics Committee) of the Faculty of Medicine, Ain Shams University (protocol code FMASU R212/2023) according to the Committee on Animal Research Ethics (CARE) under the guidelines of the Norwegian National Committee for Research Ethics in Science and Technology (NENT).

Acknowledgments

The authors extend their appreciation to the Deanship for Research & Innovation, Ministry of Education in Saudi Arabia, for funding this research through project number IFP22UQU4360890DSR241.

Author Contributions

All authors made a significant contribution to the work reported, whether that is in the conception, study design, execution, acquisition of data, analysis and interpretation, or in all these areas; took part in drafting, revising or critically reviewing the article; gave final approval of the version to be published; have agreed on the journal to which the article has been submitted; and agree to be accountable for all aspects of the work.

Disclosure

The authors declare that this research was conducted in the absence of any commercial or financial relationships that could be construed as potential conflicts of interest.

References

1. Salton F, Ruaro B, Confalonieri P, Confalonieri M. Epithelial–Mesenchymal Transition: a Major Pathogenic Driver in Idiopathic Pulmonary Fibrosis? *Medicina*. 2020;56(11):608. doi:10.3390/medicina56110608
2. Zhang C, Xi Y, Zhang Y, et al. Genetic association analysis of dietary intake and idiopathic pulmonary fibrosis: a two-sample Mendelian randomization study. *BMC Pulm Med*. 2024;24(1):15. doi:10.1186/s12890-023-02831-8
3. Martinez FJ, Collard HR, Pardo A, et al. Idiopathic pulmonary fibrosis. *Lancet*. 2017;3(1):1–19.
4. Confalonieri P, Volpe MC, Jacob J, et al. Regeneration or Repair? The Role of Alveolar Epithelial Cells in the Pathogenesis of Idiopathic Pulmonary Fibrosis (IPF). *Cells*. 2022;11(13):2095. doi:10.3390/cells11132095
5. Holland AEJJo P. Physiotherapy management of interstitial lung disease. *J Physiother*. 2022;68(3):158–164.
6. Masola V, Zaza G, Gambaro G, et al. Heparanase: a potential new factor involved in the renal epithelial mesenchymal transition (EMT) induced by ischemia/reperfusion (I/R) injury. *PLoS One*. 2016;11(7):e0160074. doi:10.1371/journal.pone.0160074

7. Tzanakakis G, Kavasi RM, Voudouri K, et al. Role of the extracellular matrix in cancer-associated epithelial to mesenchymal transition phenomenon. *Development Dyn*. 2018;247(3):368–381. doi:10.1002/dvdy.24557
8. Wicki A, Lehembre F, Wick N, Hantusch B, Kerjaschki D, Christofori G. Tumor invasion in the absence of epithelial-mesenchymal transition: podoplanin-mediated remodeling of the actin cytoskeleton. *Cancer Cell*. 2006;9(4):261–272. doi:10.1016/j.ccr.2006.03.010
9. Della Latta V, Cecchettini A, Del Ry S, Morales M. Bleomycin in the setting of lung fibrosis induction: from biological mechanisms to counteractions. *Pharmacol Res*. 2015;97:122–130. doi:10.1016/j.phrs.2015.04.012
10. Blaszczak W, Barczak W, Masternak J, Kopczyński P, Zhitkovich A, Rubiś BJM. Vitamin C as a Modulator of the Response to Cancer Therapy. *Molecules*. 2019;24(3):453. doi:10.3390/molecules24030453
11. Li D, Guabiraba R, Besnard A-G, et al. IL-33 promotes ST2-dependent lung fibrosis by the induction of alternatively activated macrophages and innate lymphoid cells in mice. *J Allergy Clin Immunol*. 2014;134(6):1422–1432.e1411. doi:10.1016/j.jaci.2014.05.011
12. Altintas N, Erboga M, Aktas C, et al. Protective effect of infliximab, a tumor necrosis factor-alfa inhibitor, on bleomycin-induced lung fibrosis in rats. *Inflammation*. 2016;39(1):65–78. doi:10.1007/s10753-015-0224-z
13. Chu Q, Gu X, Zheng Q, et al. Long noncoding RNA SNHG4: a novel target in human diseases. *Can Cell Inter*. 2021;21(1):583. doi:10.1186/s12935-021-02292-1
14. Mattick JS, Amaral PP, Carninci P, et al. Long non-coding RNAs: definitions, functions, challenges and recommendations. *Nat Rev Mol Cell Biol*. 2023;24(6):430–447. doi:10.1038/s41580-022-00566-8
15. Cai Y, Huang Y, Zhang J, et al. LncRNA CBR3-AS1 predicts a poor prognosis and promotes cervical cancer progression through the miR-3163/LASP1 pathway (0028-2685 (Print). *Neoplasma*. 2022;69:1.
16. Liu S, Zhan N, Gao C, et al. Long noncoding RNA CBR3-AS1 mediates tumorigenesis and radiosensitivity of non-small cell lung cancer through redox and DNA repair by CBR3-AS1 /miR-409-3p/SOD1 axis 1872-7980 (Electronic). *Cancer Lett*. 2022;526;1
17. Ghafouri-Fard S, Glassy MC, Abak A, Hussen BM, Niazi V, Taheri M. The interaction between miRNAs/lncRNAs and Notch pathway in human disorders. *Biomed Pharmacother*. 2021;138:111496. doi:10.1016/j.biopha.2021.111496
18. Ma F, Wang S-H, Cai Q, et al. Long non-coding RNA TUG1 promotes cell proliferation and metastasis by negatively regulating miR-300 in gallbladder carcinoma. *Biomed Pharmacother*. 2017;88:863–869. doi:10.1016/j.biopha.2017.01.150
19. Yang M, Chen W, Liu H, Yu L, Tang M, Liu Y. Long Non-coding RNA CBR3 Antisense RNA 1 is Downregulated in Colorectal Cancer and Inhibits miR-29a-Mediated Cell Migration and Invasion. *Mol Biotechnol*. 2022;64(7):773–779. doi:10.1007/s12033-021-00444-2
20. Xiao J, Meng X, Huang XR, et al. miR-29 inhibits bleomycin-induced pulmonary fibrosis in mice (1525-0024 (Electronic). *Mol Ther*. 2012;20:1251–1260.
21. Chioccioli M, Roy S, Newell R, et al. A lung targeted miR-29 mimic as a therapy for pulmonary fibrosis. *eBioMedicine*. 2022;85:104304. doi:10.1016/j.ebiom.2022.104304
22. Cushing L, Kuang PP, Qian J, et al. miR-29 Is a Major Regulator of Genes Associated with Pulmonary Fibrosis. *Am J Respir Cell Mol Biol*. 2011;45(2):287–294. doi:10.1165/rcmb.2010-0323OC
23. Zong D, Ouyang R, Li J, Chen Y, Chen P. Notch signaling in lung diseases: focus on Notch1 and Notch3. *Ther Adv Respirat Dis*. 2016;10(5):468–484. doi:10.1177/1753465816654873
24. Yuan Q, Tan RJ, YJRFM L. Myofibroblast in kidney fibrosis: origin, activation, and regulation. *Renal Fibrosis*. 2019;2019:253–283.
25. Proença C, Freitas M, Ribeiro D, Rufino AT, Fernandes E, Ferreira de Oliveira JMPJMRR. The role of flavonoids in the regulation of epithelial-mesenchymal transition in cancer: a review on targeting signaling pathways and metastasis. *Med Res Rev*. 2023;43(6):1878–1945. doi:10.1002/med.21966
26. Ricard-Blum S, Baffet G, Théret NJMB. Molecular and tissue alterations of collagens in fibrosis. *Matrix Biol*. 2018;68-69:122–149. doi:10.1016/j.matbio.2018.02.004
27. Liu X, Hu H, Yin JQJLI. Therapeutic strategies against TGF-β signaling pathway in hepatic fibrosis. *Liver Int*. 2006;26(1):8–22. doi:10.1111/j.1478-3231.2005.01192.x
28. Delaunay S, Frye M. RNA modifications regulating cell fate in cancer. *Nat Cell Biol*. 2019;21(5):552–559. doi:10.1038/s41556-019-0319-0
29. Gallorini M, Carradori SJEOo DD. Understanding collagen interactions and their targeted regulation by novel drugs. *Expert Opin Drug Discov*. 2021;16(11):1239–1260. doi:10.1080/17460441.2021.1933426
30. Brignall R, Moody AT, Mathew S, Gaudet S. Considering Abundance, Affinity, and Binding Site Availability in the NF-OεB Target Selection Puzzle. *Front Immunol*. 2019;10:10. doi:10.3389/fimmu.2019.00010
31. Mulero MC, Wang VY-F, Huxford T, Ghosh G. Genome reading by the NF-κB transcription factors. *Nuc Acids Res*. 2019;47(19):9967–9989. doi:10.1093/nar/gkz739
32. Metzemaekers M, Vanheule V, Janssens R, Struyf S, Proost P. Overview of the mechanisms that may contribute to the non-redundant activities of interferon-inducible CXC chemokine receptor 3 ligands. *Front Immunol*. 2018;8:1970. doi:10.3389/fimmu.2017.01970
33. Novick D, Kim S, Kaplanski G, Dinarello CA Interleukin-18, more than a Th1 cytokine. Paper presented at: Seminars in immunology. 2013.
34. Wolf SI, Lawson CJCADNI. Novel Approaches. Edited by Squeri A I. ICAM-1: contribution to vascular inflammation and early atherosclerosis. *Coronary Artery Dis*. 2012;2012:65–90.
35. Theocharis AD, Manou D, Karamanos N. The extracellular matrix as a multitasking player in disease. *FEBS J*. 2019;286(15):2830–2869. doi:10.1111/febs.14818
36. Kim TH, Kim S-H, Seo J-Y, et al. Blockade of the Wnt/β-catenin pathway attenuates bleomycin-induced pulmonary fibrosis. *Tohoku J Exp Med*. 2011;223(1):45–54. doi:10.1620/tjem.223.45
37. Zhao S, Xiao X, Sun S, et al. MicroRNA-30d/JAG1 axis modulates pulmonary fibrosis through Notch signaling pathway. *Pathol Res Pract*. 2018;214(9):1315–1323. doi:10.1016/j.prp.2018.02.014
38. Zhao M, Wang L, Wang M, et al. Targeting fibrosis: mechanisms and clinical trials. *Signal Transduct Target Ther*. 2022;7(1):206. doi:10.1038/s41392-022-01070-3
39. Zhang L, Ding W-Y, Wang Z-H, et al. Early administration of trimetazidine attenuates diabetic cardiomyopathy in rats by alleviating fibrosis, reducing apoptosis and enhancing autophagy. *J Transl Med*. 2016;14(1):1–12.
40. Yan Y, Xu Z, Dai S, et al. Targeting autophagy to sensitive glioma to temozolomide treatment. *J Experiment Clin Cancer Res*. 2016;35:1–14.
41. Zhou B, Lin W, Long Y, et al. Notch signaling pathway: architecture, disease, and therapeutics. *Signal Transduct Target Ther*. 2022;7(1):95. doi:10.1038/s41392-022-00934-y

42. Ding W, Zhou D, Zhang S, Qian J, Yang L, Tang L. Trimetazidine inhibits liver fibrosis and hepatic stellate cell proliferation and blocks transforming growth factor-OI (TGFOI)/Smad signaling in vitro and in vivo. *Bioengineered*. 2022;13(3):7147–7156. doi:10.1080/21655979.2022.2047403
43. Ahmed EA, Alzahrani AM. SOXC Transcription Factors as Diagnostic Biomarkers and Therapeutic Targets for Arthritis. *Int J Mol Sci*. 2023;24(4). doi:10.3390/ijms24044215
44. Mohamed DI, Ezzat SF, Elayat WM, et al. Hepatoprotective Role of Carvedilol against Ischemic Hepatitis Associated with Acute Heart Failure via Targeting miRNA-17 and Mitochondrial Dynamics-Related Proteins: an In Vivo and In Silico Study. *Pharmaceuticals*. 2022;15(7). doi:10.3390/ph15070832.
45. Mohamed DI, El-Waseef DAEDA, Nabih ES, et al. Acetylsalicylic Acid Suppresses Alcoholism-Induced Cognitive Impairment Associated with Atorvastatin Intake by Targeting Cerebral miRNA155 and NLRP3: in Vivo, and In Silico Study. *Pharmaceutics*. 2022;14(3):529. doi:10.3390/pharmaceutics14030529
46. Koch-Edelmann S, Banhart S, Saied EM, et al. The cellular ceramide transport protein CERT promotes Chlamydia psittaci infection and controls bacterial sphingolipid uptake. *Cell Microbiol*. 2017;19(10):e12752. doi:10.1111/cmi.12752
47. Wang T, Wang Z, de Fabritus L, et al. 1-deoxysphingolipids bind to COUP-TF to modulate lymphatic and cardiac cell development. *Dev Cell*. 2021;56(22):3128–3145.e3115. doi:10.1016/j.devcel.2021.10.018
48. Healey RD, Saied EM, Cong X, et al. Discovery and Mechanism of Action of Small Molecule Inhibitors of Ceramidases**. *Angew Chem Int Ed*. 2022;61(2). doi:10.1002/anie.202109967.
49. Samaha D, Hamdo HH, Cong X, et al. Liposomal FRET Assay Identifies Potent Drug-Like Inhibitors of the Ceramide Transport Protein (CERT). *Chem–Eur J*. 2020;26(70):16616–16621. doi:10.1002/chem.202003283
50. Kalinichenko LS, Mühle C, Jia T, et al. Neutral sphingomyelinase mediates the co-morbidity trias of alcohol abuse, major depression and bone defects. *Mol Psychia*. 2021;26(12):7403–7416. doi:10.1038/s41380-021-01304-w
51. Mohamed DI, Abou-Bakr DA, Ezzat SF, et al. Vitamin d3 prevents the deleterious effects of testicular torsion on testis by targeting miRNA-145 and adam17: in silico and in vivo study. *Pharmaceuticals*. 2021;14(12). doi:10.3390/ph14121222.
52. Jin C, Jia Y, Jin C, et al. Therapeutic effect of Halofuginone on ITP mice by regulating the differentiation of Th cell subsets. *Int Immunopharmacol*. 2014;18(2):213–216. doi:10.1016/j.intimp.2013.12.013
53. Pan L, Cheng Y, Yang W, et al. Nintedanib Ameliorates Bleomycin-Induced Pulmonary Fibrosis, Inflammation, Apoptosis, and Oxidative Stress by Modulating PI3K/Akt/mTOR Pathway in Mice. *Inflammation*. 2023;46(4):1531–1542. doi:10.1007/s10753-023-01825-2
54. Yang L, Chen P-P, Luo M, et al. Inhibitory effects of total ginsenoside on bleomycin-induced pulmonary fibrosis in mice. *Biomed. Pharmacother*. 2019;114:108851. doi:10.1016/j.biopha.2019.108851
55. Ji Y, Wang T, Wei Z-F, et al. Paeoniflorin, the main active constituent of Paeonia lactiflora roots, attenuates bleomycin-induced pulmonary fibrosis in mice by suppressing the synthesis of type I collagen. *J Ethnopharmacol*. 2013;149(3):825–832. doi:10.1016/j.jep.2013.08.017
56. Chen X, Xia X, Dong T, Lin Z, Du L, Zhou H. Trimetazidine Reduces Cardiac Fibrosis in Rats by Inhibiting NOX2-Mediated Endothelial-to-Mesenchymal Transition. *Drug Des Devel Ther*. 2022;16(1177–8881):2517–2527. doi:10.2147/DDDT.S360283
57. Kliment CR, Englert JM, Crum LP, Oury TD, Oury TD. A novel method for accurate collagen and biochemical assessment of pulmonary tissue utilizing one animal. *Int J Clin Exp Pathol*. 2011;4(4):349–355.
58. Ohbayashi M, Suzuki M, Yashiro Y, et al. Induction of pulmonary fibrosis by methotrexate treatment in mice lung in vivo and in vitro. *J Toxicol Sci*. 2010;35(5):653–661. doi:10.2131/jts.35.653
59. Bancroft JD, Layton C, Suvarna SK. *Bancroft's Theory and Practice of Histological Techniques*. Churchill Livingstone Elsevier; 2013.
60. Klisic A, Radoman Vujacic I, Munjas J, Ninic A, Kotur-Stevuljevic J. Micro-ribonucleic acid modulation with oxidative stress and inflammation in patients with type 2 diabetes mellitus - A review article. *AMS*. 2022;18(4):870–880. doi:10.5114/aoms/146796
61. Sun Q, Lei X, Yang X. The crosstalk between non-coding RNAs and oxidative stress in cancer progression. *Genes Dis*. 2024;101286. doi:10.1016/j.gendis.2024.101286
62. Zhang L, Wang M, Kang X, et al. Oxidative stress and asthma: proteome analysis of chitinase-like proteins and FIZZ1 in lung tissue and bronchoalveolar lavage fluid. *J Proteome Res*. 2009;8(4):1631–1638. doi:10.1021/pr800685h
63. He C, Larson-Casey JL, Gu L, Ryan AJ, Murthy S, Carter AB. Cu,Zn-superoxide dismutase-mediated redox regulation of jumonji domain containing 3 modulates macrophage polarization and pulmonary fibrosis. *Am J Respir Cell Mol Biol*. 2016;55(1):58–71. doi:10.1165/rcmb.2015-0183OC
64. Liu S, Zhan N, Gao C, et al. Long noncoding RNA CBR3-AS1 mediates tumorigenesis and radiosensitivity of non-small cell lung cancer through redox and DNA repair by CBR3-AS1 /miR-409-3p/SOD1 axis. *Cancer Lett*. 2022;526:1–11. doi:10.1016/j.canlet.2021.11.009
65. World Health Organization. *Global Health Risks: Mortality and Burden of Disease Attributable to Selected Major Risks*. World Health Organization; 2009.
66. Chanda D, Otoupalova E, Smith SR, Volckaert T, De Langhe SP, Thannickal V. Developmental pathways in the pathogenesis of lung fibrosis. *Mol Asp Med*. 2019;65:56–69. doi:10.1016/j.mam.2018.08.004
67. Liu T, De Los Santos FG, Phan SHJFM. The bleomycin model of pulmonary fibrosis. *Fibrosis*. 2017; 2017:27–42.
68. Shi K, Jiang J, Ma T, et al. Pathogenesis pathways of idiopathic pulmonary fibrosis in bleomycin-induced lung injury model in mice. *Respir Physiol Neurobiol*. 2014;190:113–117. doi:10.1016/j.resp.2013.09.011
69. Zhao W, Cheng L, Quek C, Bellingham SA, Hill AF. Novel miR-29b target regulation patterns are revealed in two different cell lines. *Sci Rep*. 2019;9(1):17449. doi:10.1038/s41598-019-53868-x
70. Liu T, Yu H, Ullenbruch M, et al. The in vivo fibrotic role of FIZZ1 in pulmonary fibrosis. *PLoS One*. 2014;9(2):e88362. doi:10.1371/journal.pone.0088362
71. Yin Q, Wang W, Cui G, Yan L, Zhang SJJo CP. Potential role of the Jagged1/Notch1 signaling pathway in the endothelial-myofibroblast transition during BLM-induced pulmonary fibrosis. *J Cell Physiol*. 2018;233(3):2451–2463. doi:10.1002/jcp.26122
72. Hou J, Ma T, Cao H, et al. TNF-α-induced NF-κB activation promotes myofibroblast differentiation of LR-MSCs and exacerbates bleomycin-induced pulmonary fibrosis. *J Cell Physiol*. 2018;233(3):2409–2419. doi:10.1002/jcp.26112
73. Zank DC, Bueno M, Mora AL, Rojas M. Idiopathic pulmonary fibrosis: aging, mitochondrial dysfunction, and cellular bioenergetics. *Front Med*. 2018;5:10. doi:10.3389/fmed.2018.00010
74. Zhang H, Liu M, Zhang Y, Li X, Zhou W. Trimetazidine Attenuates Exhaustive Exercise-Induced Myocardial Injury in Rats via Regulation of the Nrf2/NF-ΟcB Signaling Pathway. *Front Pharmacol*. 2019;10:10. doi:10.3389/fphar.2019.00010

75. Pourfarzam S, Ghazanfari T, Yaraee R, et al. Serum levels of IL-8 and IL-6 in the long term pulmonary complications induced by sulfur mustard: sardasht-Iran Cohort Study. *Int Immunopharmacol*. 2009;9(13–14):1482–1488. doi:10.1016/j.intimp.2009.09.002
76. Shijubo N, Imai K, Aoki S, et al. Circulating intercellular adhesion molecule-1 (ICAM-1) antigen in sera of patients with idiopathic pulmonary fibrosis. *Clin Experiment Immunol*. 1992;89(1):58–62. doi:10.1111/j.1365-2249.1992.tb06877.x
77. Shijubo N, Imai K, Shigehara K, et al. Soluble intercellular adhesion molecule-1 (ICAM-1) in sera and bronchoalveolar lavage fluid of patients with idiopathic pulmonary fibrosis and pulmonary sarcoidosis. *Clin Experiment Immunol*. 1994;95(1):156–161. doi:10.1111/j.1365-2249.1994.tb06030.x
78. Theocharis AD, Skandalis SS, Gialeli C, Karamanos N. Extracellular matrix structure. *Adv Drug Deliv Rev*. 2016;97:4–27.
79. Yasmina B, Eric SW, Simon de B, et al. MMP-7 is a predictive biomarker of disease progression in patients with idiopathic pulmonary fibrosis. *ERJ Open Res*. 2017;3(1):00074–02016. doi:10.1183/23120541.00074-2016
80. Aoshima Y, Enomoto Y, Muto S, et al. Gremlin-1 for the differential diagnosis of idiopathic pulmonary fibrosis versus other interstitial lung diseases: a clinical and pathophysiological analysis. *Lung*. 2021;199(3):289–298. doi:10.1007/s00408-021-00440-y
81. Zhao Y, Li S, Quan E, et al. Trimetazidine inhibits cardiac fibrosis by reducing reactive oxygen species and downregulating connective tissue growth factor in streptozotocinвЂ'induced diabetic rats. *Exp Ther Med*. 2019;18(2):1477–1485. doi:10.3892/etm.2019.7705
82. Manoury B, Caulet-Maugendre S, Guénon I, Lagente V, Boichot E. Boichot EJIjoi, pharmacology. TIMP-1 is a key factor of fibrogenic response to bleomycin in mouse lung. *Int J Immunopathol Pharmacol*. 2006;19(3):471–487. doi:10.1177/039463200601900303
83. Yukselen V, Onder Karaoglu A, Yenisey C, Tuncyurek M, Ozutemiz O. Trimetazidine reduces the degree of fibrosis in alkali burns of the esophagus. *J Pediatr Surg*. 2005;40(3):505–509. doi:10.1016/j.jpedsurg.2004.11.036
84. Reinert T, Baldotto C, Nunes FAP, Scheliga AA. Bleomycin-induced lung injury. *J Cancer Res*. 2013;2013:480608
85. Liu M-H, Lin A-H, H-K K, Perng D-W, Lee T-S, YRJFip K. Prevention of bleomycin-induced pulmonary inflammation and fibrosis in mice by paeonol. *Front Physiol*. 2017;8:193. doi:10.3389/fphys.2017.00193
86. Kumar K, St GW, Lykke A. Pulmonary responses to bleomycin-induced injury: an immunomorphologic and electron microscopic study. *Experiment Pathol*. 1985;28(1):33–43.
87. Allawzi A, Elajaili H, Redente EF, Nozik-Grayck E. Oxidative toxicology of bleomycin: role of the extracellular redox environment. *Curr Opin Toxicol*. 2019;13:68–73. doi:10.1016/j.cotox.2018.08.001
88. Razzaque M, Hossain M, Kohno S, Taguchi TJVA. Bleomycin-induced pulmonary fibrosis in rat is associated with increased expression of collagen-binding heat shock protein (HSP) 47. *Virchows Archiv*. 1998;432(5):455–460. doi:10.1007/s004280050191
89. Sousa AM, Liu T, Guevara O, et al. Smooth muscle α-actin expression and myofibroblast differentiation by TGFβ are dependent upon MK2. *J Cell Biochem*. 2007;100(6):1581–1592. doi:10.1002/jcb.21154
90. Weng C-M, Li Q, Chen K-J, et al. Bleomycin induces epithelial-to-mesenchymal transition via bFGF/PI3K/ESRP1 signaling in pulmonary fibrosis. *Biosci Rep*. 2020;40(1):BSR20190756. doi:10.1042/BSR20190756